sensors

MDPI

Review

Chemoresistive Gas Sensors Based on Electrospun 1D Nanostructures: Synergizing Morphology and Performance Optimization

Aigerim Imash [1,2], Gaukhar Smagulova [1,*], Bayan Kaidar [1], Aruzhan Keneshbekova [1,3], Ramazan Kazhdanbekov [2], Leticia Fernandez Velasco [4] and Zulkhair Mansurov [1,2]

[1] Institute of Combustion Problems, 172 Bogenbay Batyr Str., Almaty 050012, Kazakhstan; imash.aigerim@icp.kz (A.I.); kaidar.bayan@icp.kz (B.K.); a.keneshbekova@icp.kz (A.K.); zmansurov@kaznu.kz (Z.M.)

[2] Faculty of Chemistry and Chemical Technology, Al Farabi Kazakh National University, 71 al-Farabi Ave., Almaty 050040, Kazakhstan; kazhdanbekov_ramazan@live.kaznu.kz

[3] International Chinese-Belorussian Scientiffc Laboratory on Vacuum Plasma Technology, Nanjing University of Science and Technology, 200 Xiaolingwei str., Nanjing 210094, China

[4] Department of Chemistry, Royal Military Academy, Avenue de la Renaissance 30, 1000 Brussels, Belgium; leti_fv@hotmail.com

* Correspondence: smagulova.gaukhar@gmail.com; Tel.: +7-7075666345

Abstract: Gas sensors are essential for safety and quality of life, with broad applications in industry, healthcare, and environmental monitoring. As urbanization and industrial activities intensify, the need for advanced air quality monitoring becomes critical, driving the demand for more sensitive, selective, and reliable sensors. Recent advances in nanotechnology, particularly 1D nanostructures like nanofibers and nanowires, have garnered significant interest due to their high surface area and improved charge transfer properties. Electrospinning stands out as a promising technique for fabricating these nanomaterials, enabling precise control over their morphology and leading to sensors with exceptional attributes, including high sensitivity, rapid response, and excellent stability in harsh conditions. This review examines the current research on chemoresistive gas sensors based on 1D nanostructures produced by electrospinning. It focuses on how the morphology and composition of these nanomaterials influence key sensor characteristics—sensitivity, selectivity, and stability. The review highlights recent advancements in sensors incorporating metal oxides, carbon nanomaterials, and conducting polymers, along with their modifications to enhance performance. It also explores the use of fiber-based composite materials for detecting oxidizing, reducing, and volatile organic compounds. These composites leverage the properties of various materials to achieve high sensitivity and selectivity, allowing for the detection of a wide range of gases in diverse conditions. The review further addresses challenges in scaling up production and suggests future research directions to overcome technological limitations and improve sensor performance for both industrial and domestic air quality monitoring applications.

Keywords: chemoresistive gas sensors; electrospinning; 1D nanostructured materials; composites; electrospun fibers

Citation: Imash, A.; Smagulova, G.; Kaidar, B.; Keneshbekova, A.; Kazhdanbekov, R.; Velasco, L.F.; Mansurov, Z. Chemoresistive Gas Sensors Based on Electrospun 1D Nanostructures: Synergizing Morphology and Performance Optimization. *Sensors* **2024**, *24*, 6797. https://doi.org/10.3390/s24216797

Academic Editor: Pengcheng Xu

Received: 19 September 2024
Revised: 7 October 2024
Accepted: 15 October 2024
Published: 23 October 2024

1. Introduction

Gas sensors are indispensable in modern life, ensuring both safety and a higher quality of living [1]. As urbanization and industrialization accelerate, monitoring air quality has become more crucial than ever. In industrial settings, gas sensors help prevent accidents and detect toxic leaks, while in the automotive sector, they contribute to reducing harmful emissions [2,3]. In healthcare, these sensors facilitate early disease diagnosis through breath analysis [4], and in everyday life, they help maintain safer environments by continuously monitoring air quality. For gas sensors to be effective they must exhibit high sensitivity for detecting low gas concentrations [5], excellent selectivity to distinguish between various

gases [6], and fast response and recovery times [7]. They also need to be stable and durable under different environmental conditions [8,9], consume minimal power, and be easily integrated into electronic systems [10].

The graph below illustrates the number of publications on gas sensors from 1980 to 2023, based on data from the Scopus database (see Figure 1). A sharp rise in publications since the early 21st century indicates a significant increase in scientific interest and research activity in this field. This surge is driven by the growing demand for more efficient and reliable sensors to meet challenges in industries such as manufacturing, healthcare, and environmental protection. Technological advancements, particularly the use of 1D nanostructures, have greatly enhanced the performance of gas sensors, which is reflected in the rising number of studies and publications in this area.

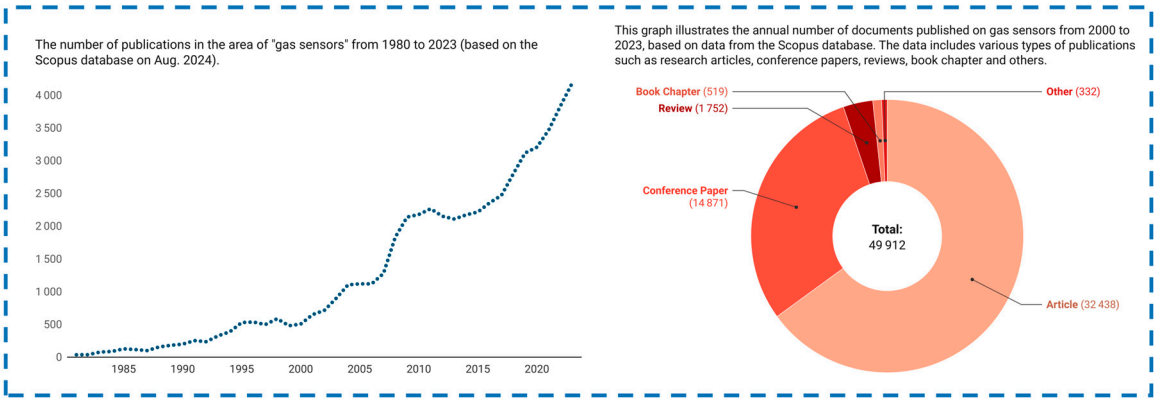

Figure 1. The number of publications on gas sensors from 1980 to 2023, based on data from the Scopus database.

Gas sensors vary in their transduction mechanisms and include optical [11], electrochemical [12], electrical [13], and piezoelectric sensors [14]. Chemoresistive gas sensors belong to the electrical type of transduction, detecting and quantifying gaseous analytes by measuring changes in their electrical resistance. The primary working principle of chemoresistive sensors is based on the adsorption and desorption of gas molecules on the surface of the sensing material, which alters the charge carrier density and, consequently, the material's electrical resistance [15]. The interaction of gas molecules with active centers on the surface changes the energy barrier for charge carrier movement, which forms the basis of the measurable signal.

Chemoresistive gas sensors can be classified according to various criteria, such as the type of sensing material, detection method, and application area. Based on the materials used, these sensors are divided into several categories: semiconductor metal oxide (SMOx)-based sensors [16], carbon-based materials [17], conductive polymers [18], and composites [19]. SMOx, such as SnO_2, ZnO, and TiO_2, are the most commonly used materials due to their high sensitivity and stability [20–22]. Carbon-based materials, like carbon nanotubes, graphene, and reduced graphene oxide (rGO), have gained attention for their unique electrical and mechanical properties [23]. Conductive polymers, such as polyaniline (PANI) and polypyrrole (PPy), are also used because of their flexibility and modifiability [24]. Composites, which combine different materials, offer enhanced sensor performance due to synergistic effects [25].

Various methods are employed to fabricate chemoresistive gas sensors, including chemical deposition [26], spray pyrolysis [27], sol-gel processing [28], and electrospinning (ES) [29,30]. Each method offers its own advantages and limitations depending on the desired sensor characteristics. One of the most versatile and cost-effective methods is electrospinning. This process involves applying a high voltage to a polymer solution or melt, resulting in the formation of a thin jet that elongates and solidifies into fibers as it moves toward a grounded collector [31]. The resulting nanofibers can be assembled into

nonwoven mats or aligned arrays, depending on the collector configuration [32]. One of the key advantages of electrospinning is the ability to produce fibers with diameters ranging from tens of nanometers to several micrometers, enabling precise control over the material's morphology to suit specific applications [33].

Advantages of 1D nanostructures, such as nanofibers and nanowires, include enhanced diffusion properties and efficient charge transport, which provide more active centers for gas adsorption compared to 2D and 3D nanostructures [34]. Their high aspect ratio, surface energy, and unique morphology contribute to improved sensor performance, including faster response times and lower detection limits [35].

Traditional gas sensors often face challenges such as low selectivity, slow response time, and instability in harsh environments [36]. Innovative sensors based on nanomaterials can address these issues, but they also encounter challenges such as the complexity of scaling production processes and material structure heterogeneity.

This review aims to provide a comprehensive analysis of current research on chemoresistive gas sensors utilizing 1D nanostructured materials fabricated by electrospinning. It will cover the fundamental principles and mechanisms of chemoresistive gas sensing, focusing on the influence of material morphology and composition on sensor properties; detail the electrospinning process and parameters affecting nanofiber structure and properties; review various materials used in electrospun gas sensors, such as metal oxides, carbon materials, conducting polymers, and composites, with examples from recent literature; examine post-annealing methods and modifications aimed at enhancing performance, emphasizing structural and chemical changes; offer a comparative analysis of different electrospun nanofiber gas sensors, including case studies from recent research, highlighting key factors influencing efficiency; and identify current challenges and propose future research directions to overcome existing limitations and improve sensor performance.

2. Basics of Chemoresistive Gas Sensors

Chemoresistive gas sensors can be categorized into n-type and p-type based on the primary charge carriers, which can be electrons or holes. They operate on the principle of gas interaction with these charge carriers in semiconductor materials, where the donor or acceptor properties of the gases alter the charge carrier concentration through adsorption and desorption processes on the sensor surface, as well as interactions with defects or active centers. The adsorption of oxidizing gases on n-type semiconductor surfaces reduces the concentration of charge carriers and increases resistance [37], whereas reducing gases release trapped electrons, thereby decreasing resistance [38].

2.1. Operating Principles of Gas Sensors

The primary mechanisms of sensor response include ionosorption of oxygen and redox reactions on the surface of materials such as SMOx [39–41]. During ionosorption, oxygen molecules adsorb onto the surface of SMOx, forming oxygen ions (O_2^-, O^-, O^{2-}) depending on the sensor's operating temperature. For instance, at temperatures below 200 °C, O_2^- predominates, whereas at temperatures above 250 °C, O^- and O^{2-} become more prevalent due to the dissociation of oxygen molecules and the capture of electrons from the conduction band [42]. These ionic forms of oxygen alter the electrical properties of the material, generating the sensor signal. Additionally, electrostatic interactions with ionic centers on the surface, such as metal cations, enhance oxygen adsorption and influence sensor sensitivity [43].

In n-type semiconductors, an electron-depleted surface layer (EDL) forms due to the extraction of electrons from the conduction band, while in p-type semiconductors, a hole-accumulation layer (HAL) develops due to the increased concentration of holes [44]. The polarity of the sensor response, which depends on the dominant charge carriers, significantly affects its sensitivity (see Figure 2).

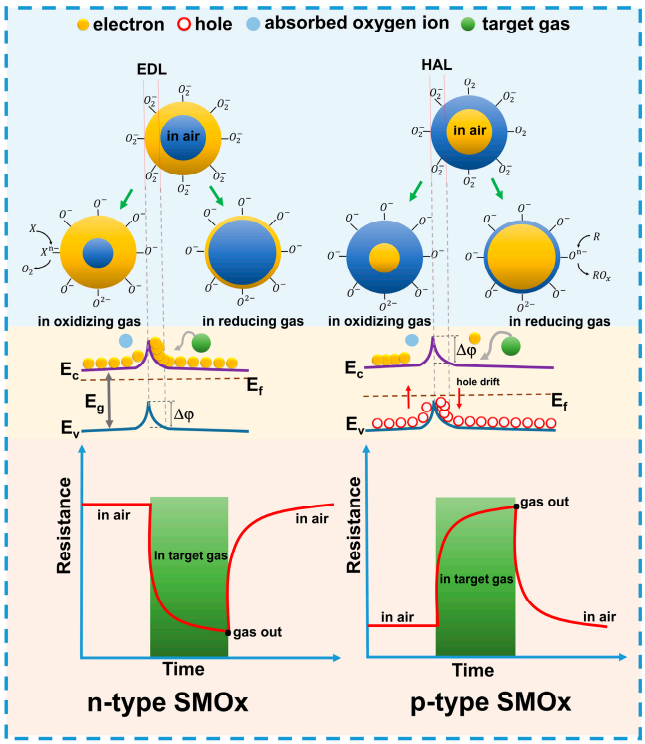

Figure 2. Schematic illustration of the mechanism of interaction of gases with electrons and holes in semiconductor metal oxides.

In the presence of oxidizing gases, the resistance of n-type semiconductors increases due to the expansion of the EDL. Conversely, in the presence of reducing gases, the resistance decreases because of the contraction of the EDL and the return of electrons to the conduction band, which enhances conductivity and alters the bending of the energy bands at the grain boundaries of the material [45]. Oxygen adsorption and reactions with gases can also affect the height of the Schottky barrier, thereby altering the conductivity and, consequently, the resistance of the sensor [46]. It is important to note that oxygen ionosorption plays a crucial role in the sensor response mechanism, and this process can be enhanced by increasing the surface area and concentration of charged metal ions on the surface [47]. The magnitude of the resistive response is determined by the intensity of surface reactions and the number of active centers, such as oxygen vacancies, which facilitate gas adsorption and change the electrical properties of the material [48].

The surface of metal oxide materials (SMOx) used in gas sensors contains various acid-base centers that play a crucial role in the gas-detection process [49]. Lewis acidic centers, represented by coordinatively unsaturated metal cations, can accept electron pairs from gas molecules, while Lewis basic centers, consisting of lattice oxygen anions, donate electron pairs. Brønsted acidic centers, formed by bridging hydroxyl (OH) groups, can donate protons to gas molecules, whereas Brønsted basic centers accept protons [50]. The presence of terminal hydroxyl groups, resulting from the dissociative adsorption of water, also influences the sensitivity of metal oxides. Managing the concentration and nature of these centers allows for the optimization of sensor sensitivity and selectivity, thereby significantly enhancing their effectiveness in gas detection [51].

It is worth noting that different gases may interact with the acid-base centers through various mechanisms, and the nature of these interactions can be predicted using Pearson's hard and soft acids and bases (HSAB) theory [52,53]. According to this theory, soft bases, such as reducing gases (e.g., hydrogen, ammonia), preferentially interact with soft acidic centers, while hard bases (e.g., oxidizing gases) interact with hard acidic centers [54]. This can serve as a useful tool in the design and optimization of gas sensor architecture to improve their performance characteristics.

2.2. Gas Sensor Performance Characteristics

Key characteristics that determine the effectiveness of gas sensors include sensitivity, selectivity, response time, and stability (see Table 1). These parameters are crucial for the development and application of sensors, ensuring their reliability and accuracy [55,56]. Sensitivity (indicated as R) is defined as the ratio of the sensor's resistance in the presence of gas (R_{gas}) to its resistance in clean air (R_{air}). For a sensor to function effectively, this ratio should be greater than 1. Selectivity is expressed as the ratio of the sensor's response to different gases. Response time is characterized by the period required for the sensor to reach 90% of the final value between R_{air} and R_{gas}, while recovery time determines how quickly the sensor returns to 90% of this value. It is also important to note that the limit of detection is a significant parameter for gas sensors, as it defines the minimum detectable concentration of a gas [57,58]. Optimizing these factors ensures measurement accuracy.

Table 1. Main characteristics of gas sensors.

Characteristics	Operating Principle	Major Limitations	Potential Solutions
Sensitivity	- Change of electrical conductivity of the conductor layer during gas adsorption - Change in mass of the sensing element (for piezoelectric sensors) - Optical absorption (for optical sensors)	- Low signal-to-noise ratio for trace gases - Interference from other gases - Influence of temperature and humidity	- Nanostructured materials (e.g., SnO_2 ZnO nanoparticles [59,60]) - Noble metal alloying (e.g., Pd, Au) [61,62] - Composite materials (e.g., $ZnO@CO_3O_4$ [63]) - Optimization of the operating temperature [64,65]
Selectivity	- Specific chemical reactions on the sensor surface - Size matching between pores and gas molecules - Differences in adsorption/desorption kinetics for different gases	- Cross-sensitivity to similar gases - Difficulty in distinguishing between homologous gases (e.g., CO and H_2)	- Functionalisation by specific catalysts [66] - Selective filter membranes (e.g., ZIF-8 [67]) - Composite materials with opposite responses (e.g., SnO_2-NiO for VOCs [68])
Response time	- Adsorption/desorption rate of gas on the sensor surface - Gas diffusion rate in porous material - Rate of chemical reaction on the surface	- Slow adsorption/desorption kinetics - Diffusion limitations in porous materials	- Nanostructured materials with high specific surface area [69] - Optimization of operating temperature [70] - Thin sensing layers [71] - Catalytic additives for reaction acceleration [72]
Stability	- Preservation of physicochemical properties of the sensing layer in time - Reversibility of adsorption/desorption processes - Stability to environmental changes	- Drift of readings over time - Poisoning by interfering gases - Degradation at high temperatures	- Protective coatings (e.g., PMMA membranes) [73] - Stable nanostructures (e.g., 1D nanowires [74,75]) - Periodic recalibration [76,77]

Additionally, it is important to note that the performance of gas sensors is directly influenced by environmental conditions such as temperature and humidity, which can significantly affect gas adsorption processes on the sensor's surface [78,79]. To minimize these impacts, various methods are employed, including the use of filters or temperature control systems [73,80]. Durability is also a critical factor, as many sensors are prone to degradation and aging due to exposure to harsh environments or contamination [81]. Utilizing materials with high resistance to external conditions, as well as protective coatings, helps extend the

lifespan of sensors, ensuring their reliability and stable operation throughout their service life [82].

2.3. Materials Used in the Manufacture of Gas Sensors

The choice of sensing material is essential for optimizing the sensitivity, selectivity, and stability of gas sensors. Among the most widely utilized materials are ZnO, TiO_2, SnO_2, and WO_3, each offering distinct advantages for different sensing applications [83,84]. They exhibit high sensitivity and stability in detecting various gases [85]. However, a limitation is their requirement to operate at high temperatures (>300 °C), which increases energy consumption [86]. To enhance the performance of oxide sensors, nanostructured materials such as nanowires [87], nanotubes [88], and nanosheets [89] have been developed, which increase surface area and improve gas diffusion [90]. For example, modifying ZnO with platinum or palladium (Pd) significantly enhances sensitivity due to the sensitizing effect and catalytic activity of the surface. On the other hand, conducting polymers like PPy and PANI are widely used for creating gas sensors. These materials are attractive due to their flexibility, low cost, and ability to operate at room temperature [91,92]. Polymers can be further enhanced by incorporating metals such as gold (Au) or platinum (Pt), which increase sensitivity through greater active surface area and catalytic activity [93]. Polymers can also be used in composites with carbon nanomaterials, improving gas-sensing properties. Transition metal dichalcogenides (TMDs), such as MoS_2 and WS_2, are of interest due to their two-dimensional structure and high specific surface area, making them ideal for detecting various gases [94]. These materials offer high sensitivity and stability, particularly for detecting toxic gases like NO_2 and CO_2 [95]. When combined with nanomaterials such as graphene, TMDs show enhanced performance due to synergistic effects. Recently, MXenes have garnered significant attention among two-dimensional materials, demonstrating high sensitivity to various gases and ease of functionalization to improve selectivity and stability [96,97]. Perovskites, such as $LaCoO_3$ and $SrTiO_3$, alter their electronic structure upon gas interaction, enhancing their sensitivity. For instance, the perovskite Cs_3CuBr_5 has shown high sensitivity to gases including hydrogen and ammonia [98]. Metal–organic frameworks (MOFs), such as ZIF-8 and MIL-101, are notable for their porous structure and large specific surface area [99–101]. These materials can be functionalized to enhance selectivity for target gases and exhibit high stability even in high humidity conditions [102].

2.4. One-Dimensional Nanostructures for Gas Sensors

One-dimensional materials such as nanotubes, nanofibers, and nanowires possess unique properties that distinguish them from traditional powders and films used in gas sensors [103–105]. Firstly, due to their linear geometry and high specific surface area, 1D nanomaterials provide enhanced charge transport, leading to increased sensor sensitivity [106]. This enables them to interact more effectively with target gases, resulting in a stronger response compared to 0D and 2D materials. Secondly, 1D structures can create shorter pathways for electron transport, which minimizes the sensor's response time and improves its dynamic characteristics [107].

Recent research in the field of gas sensors has demonstrated the development of new materials and nanostructures that significantly improve sensor characteristics such as sensitivity, selectivity, and stability. For example, hollow SnO_2 nanospheres have shown a significant increase in response to hydrogen, with response and recovery times of 56 and 216 s, respectively, at 100 ppm [108]. Meanwhile, thin SnO_2 films have demonstrated a maximum response to ethanol at a concentration of 50 ppm, with response and recovery times of 259 and 214 s, respectively [109]. SnO_2 nanofibers, synthesized through electrospinning, provided the fastest response and recovery—2 and 64 s to acetone at a concentration of 50 ppm [110]. This can be attributed to the structured pathway and orientation of electron transport in the fibers, whereas in 0D and 2D materials, this process can be disrupted due to the presence of multiple directional axes. These results highlight that materials of the

same nature can yield different outcomes depending on their structure, deepening our understanding of electron transport processes (Figure 3a–c).

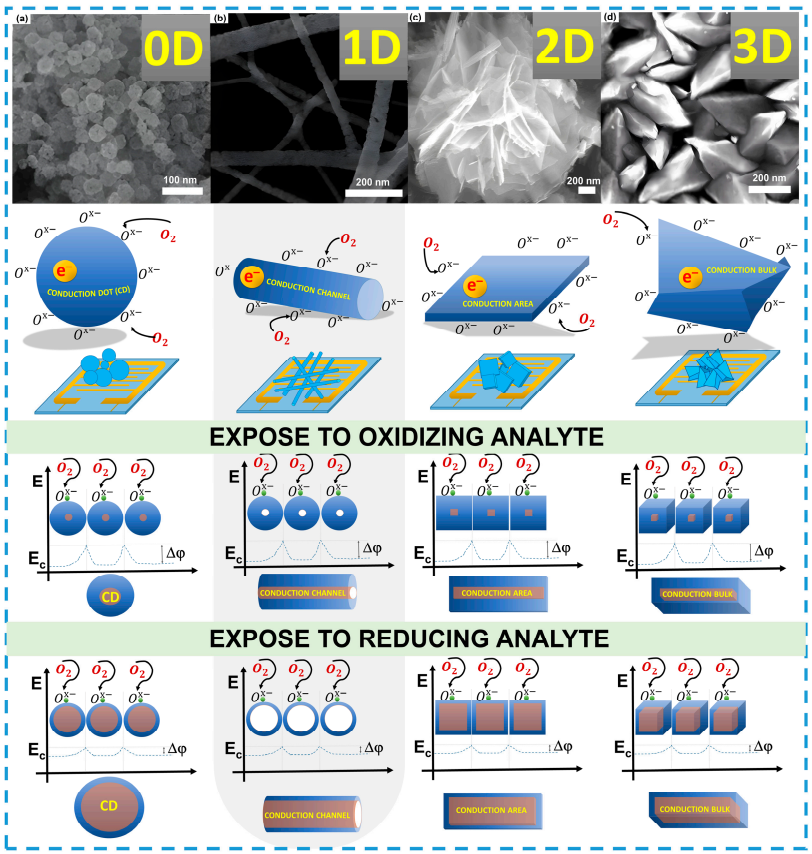

Figure 3. Mechanisms of electronic transport in nanomaterials of different dimensionalities. zero-dimensional nanospheres (**a**), reprinted with permission from Ref. [108]. One-dimensional nanofibers (**b**), reprinted with permission from Ref. [111]. Two-dimensional nanoflowers (**c**), reprinted with permission from Ref. [112]. Three-dimensional nanostructures (**d**), reprinted with permission from Ref. [109] during interaction with analytes.

A comparison with other ZnO nanostructures, such as star-shaped and spherical particles, further confirms the advantages of nanofibers. For instance, star-shaped and spherical particles show response and recovery times of 25 and 150 s, respectively, to CO at a concentration of 200 ppm [113], while nanofibers demonstrate a rapid response (25–29 s) and recovery (12–17 s) to CO in the range of 1 to 20 ppm [114]. This indicates that during the interaction with nanofibers, the conductive channel facilitates rapid electron transport (Figure 3b). In the case of 3D structures, disordered morphology can obstruct electron transport due to the high potential at grain boundaries (Figure 3b,d), which can also occur when interacting with oxidizing gases. The interaction of oxygen, as an oxidizing gas, reduces the conductive channel, increasing the potential barrier for electrons and, consequently, raising the resistance. Unlike 0D and 2D structures, linear structures provide a more uniform distribution of the conductive channel, leading to more predictable changes in resistance (Figure 3).

Thus, the use of composite and hybrid materials, as well as the development of 1D nanostructures, opens new horizons for creating highly efficient gas sensors that can meet the requirements of a wide range of applications. These advancements underscore the need for further research in the field of nanomaterials to enhance sensor characteristics and expand their functionality.

3. Fundamentals of the Electrospinning Technique

ES is a key technology for synthesizing 1D nanomaterials, such as nanofibers, with diameters ranging from nanometers to micrometers [115,116]. This method allows for the creation of materials with unique properties by precisely controlling the morphology and structure of the fibers. By varying the composition of polymeric or composite solutions and adjusting process parameters (see Figure 4), such as applied voltage, solution feed rate, the distance between the needle and collector, and the type of collector used (static or rotating), one can control the size, porosity, alignment, and orientation of the fibers [117–119].

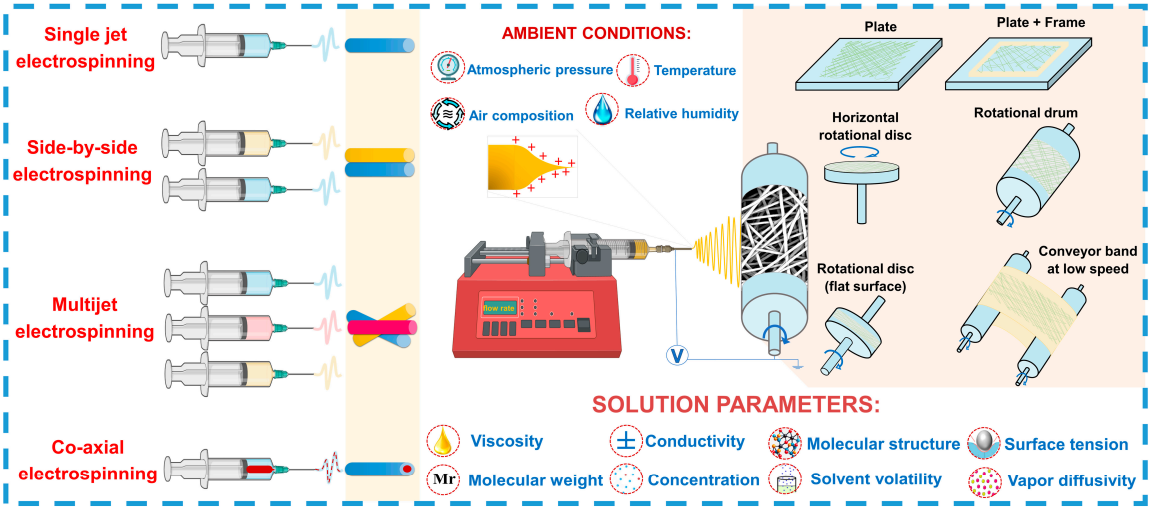

Figure 4. Schematic illustration of the electrospinning process.

Furthermore, electrospinning enables the incorporation of various additives, including nanoparticles, catalytic agents, and other functional components, which opens opportunities for creating multifunctional materials with enhanced mechanical, electrical, and chemical properties [120].

The principle of the electrospinning process is based on the stretching of a polymer solution under the influence of an electrostatic field, during which solvent evaporation occurs, and fibers are deposited onto the collector. The stability of the Taylor cone, which determines the diameter and morphology of the fibers, is critical for producing high-quality nanofibers [121]. Instability of the cone can lead to non-uniformity or the formation of globular structures. Conversely, the cone's height directly affects fiber diameter, allowing process optimization, as demonstrated in the work using polyvinylidene fluoride (PVDF) as the fiber-forming polymer under specific parameters: feed rate of 1 mL/h, voltage of 10.8 kV, and a distance of 10 cm [122,123].

In addition to cone stability, electrospinning is susceptible to various instabilities, such as axisymmetric Rayleigh instability, which results in bead-like fibers. In a recent study [124], the authors demonstrated that increasing voltage or polymer concentration helps reduce these instabilities (see Figure 5a–c). While slower solvent evaporation facilitates the formation of thinner fibers, residual charges can limit the mat's thickness to 0.5–1 mm [125]. Viscosity, polymer molecular weight, and the concentration of the fiber-forming agent also critically influence nanofiber morphology, determining their diameter and structure [126,127]. Increasing viscosity and air pressure promotes the formation of thin, uniform fibers [128]. However, surface tension of the polymer solution plays an equally important role: high surface tension induces instabilities, whereas reducing it improves fiber uniformity. The use of solvents with low surface tension and the addition of surfactants further enhance fiber morphology [129,130]. Additionally, the solution's pH significantly affects fiber size and morphology. At pH 2.6, thinner and more uniform fibers are formed compared to pH 8.5 (see Figure 5d–f) [131].

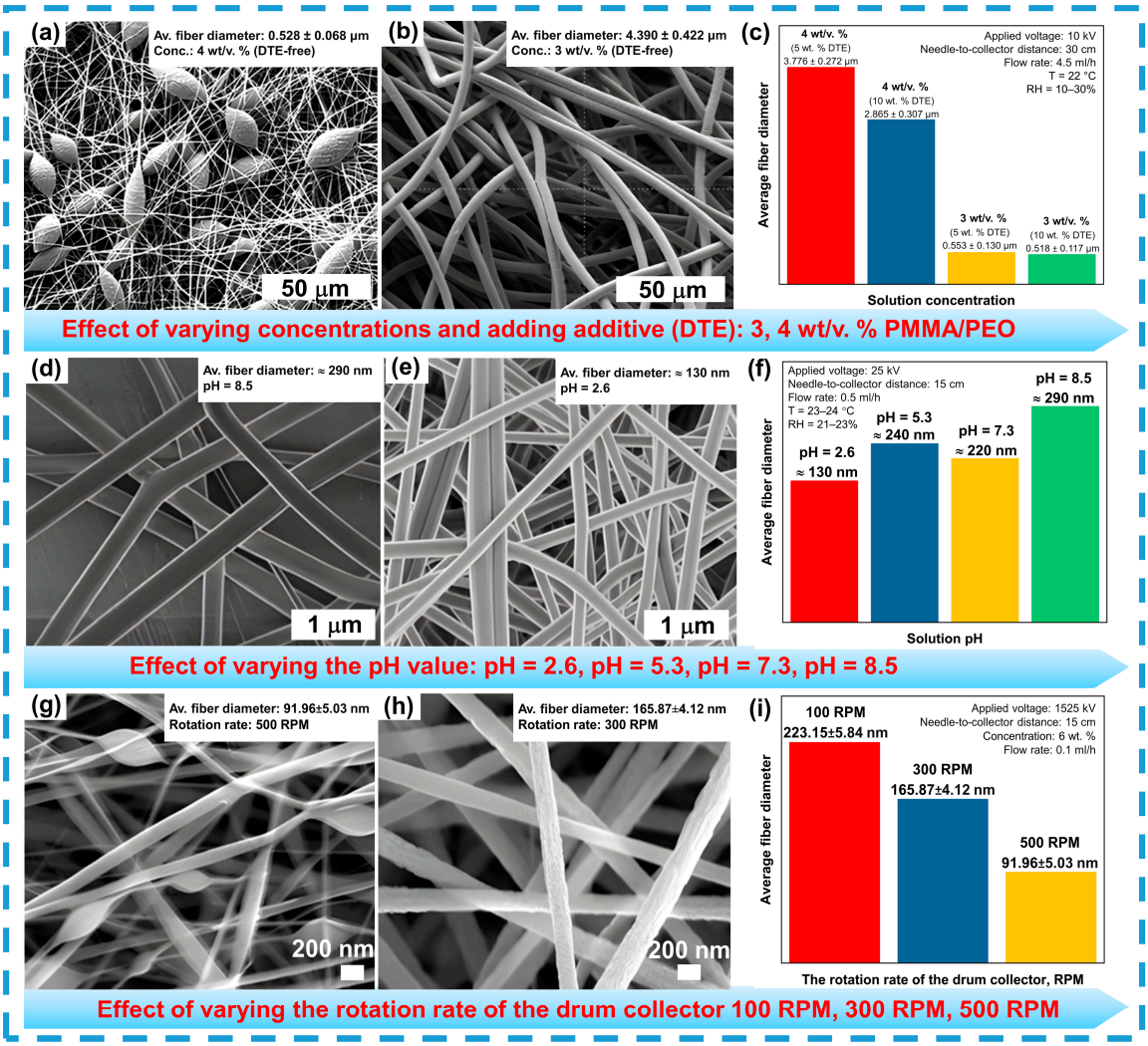

Figure 5. Effect of different conditions on nanofiber morphology and diameter: solution concentration (**a**–**c**), reprinted with permission from Ref. [124]. Solution's pH (**d**–**f**), reprinted with permission from Ref. [131]. Collector speed (**g**–**i**), reprinted with permission from Ref. [132].

One study [133] demonstrated that the geometry of the collector also affects fiber morphology: a cylindrical collector provides better tension, while a disk-shaped one results in a higher Young's modulus. The applied voltage plays a key role in the formation of the Taylor cone and the ejection of the polymer jet. For example, increasing the voltage enhances fiber stability and reduces deviations [134,135]. The collector's rotation speed also influences fiber diameter. At low speeds (100 rpm), fibers are less stretched and form irregular structures, whereas increasing the speed to 500 rpm results in more uniform fiber distribution and reduced diameters (see Figure 5g–i) [132].

Controlling the flow rate of the polymer solution is critical for achieving the desired fiber morphology. While reducing the flow rate leads to thinner fibers (see Figure 6a–c) [136], increasing it can cause the formation of beads if the flow rate becomes too high [31,137]. The applied voltage during electrospinning significantly influences the diameter and morphology of the fibers. At low voltages, globular structures tend to form due to insufficient electric field strength to produce uniform fibers. The low charge at the needle tip and the collector results in jet instability and fiber structure variations. Doubling the voltage helps produce smoother and more uniform fibers (see Figure 6d–f) [138]. Additionally, the relative humidity of the environment has a significant impact on fiber morphology. Under high humidity (65%), fibers become porous and irregular, and their diameter in-

creases. In low-humidity conditions (5%), fibers are smoother and defect-free, making their morphology more suitable for further applications (see Figure 6g–i) [139].

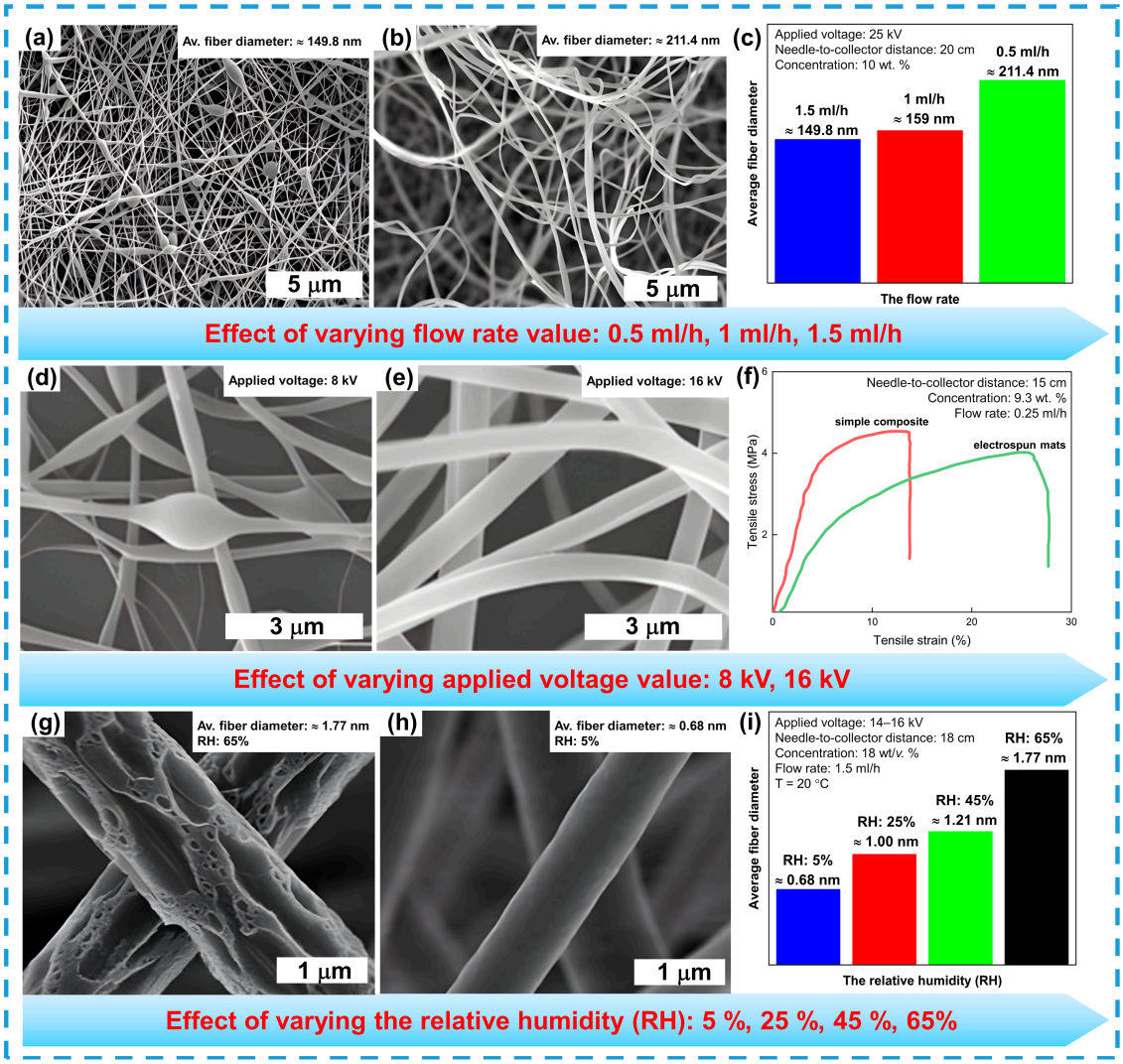

Figure 6. Effect of different conditions on nanofiber morphology: flow rate (**a**–**c**), reprinted with permission from Ref. [136]. Applied voltage (**d**–**f**), reprinted with permission from Ref. [138]. Relative humidity (**g**–**i**), reprinted with permission from Ref. [139].

On the other hand, the distance between the needle and the collector also affects the diameter and morphology of the fibers. Increasing the distance promotes the formation of thinner fibers due to enhanced stretching forces. However, if the distance is too short, thicker fibers with bead-like structures may form. Optimizing this parameter is essential to obtain high-quality fibers [140].

The addition of nanomaterials such as fullerenes, carbon nanotubes, and graphene can significantly alter the morphology of the fibers, increasing their porosity and diameter, though this may reduce the specific surface area. However, post-annealing methods like sintering can improve the mechanical properties of the fibers without altering the base polymer [141].

For gas sensors to function effectively, the length and morphology of the nanofibers are crucial, as they influence the formation of conductive channels and the resistance response during gas interaction. Unlike 2D and 3D structures, 1D nanomaterials provide optimal charge transfer, minimizing losses. Fiber diameter, grain size, and crystallinity also play a key role: reducing the diameter increases the surface area, and decreasing grain size to

the Debye radius maximizes the resistance change during gas interaction. The balance between graininess and crystallinity is critical for achieving optimal sensor sensitivity and stability [142].

4. Performance of Chemoresistive Gas Sensors Obtained by the ES Method

High sensitivity and short response time are key characteristics of gas sensors. Electrospun nanofibers, due to their high porosity and networked structure, enable efficient transport of analytes to the surface of the sensing material, significantly accelerating the sensor's response time [143,144]. The advantage of the electrospinning method lies in its relative simplicity and cost-effectiveness, making the production of such nanofibers feasible for large-scale applications. Additionally, the recyclability of nanofibers contributes to sustainable resource use and reduces environmental impact [145]. To achieve optimal gas sensor performance, careful control over both the fiber morphology and the fabrication conditions is essential [111,146].

The process of making chemoresistive sensors based on electrospun nanofibers involves several key steps. The first step is to prepare the electrospinning solution, where the choice of components such as polymers, solvents, and sensing materials determine the final properties of the fibers, followed by the electrospinning process (see Figure 7).

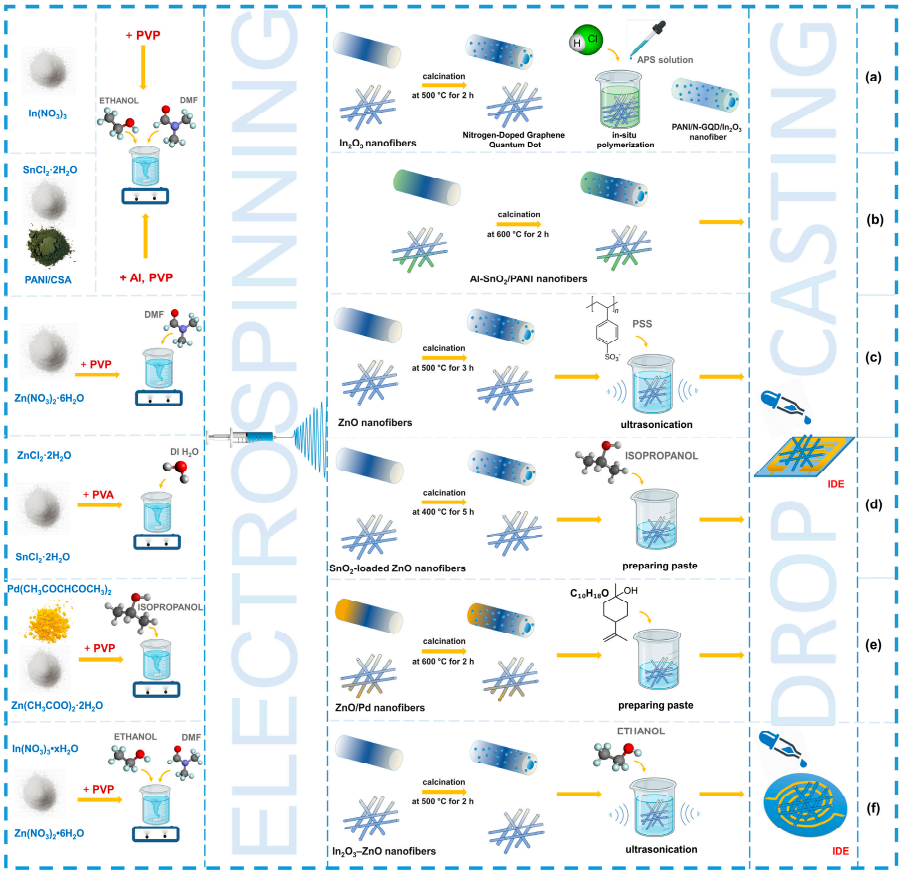

Figure 7. Fabrication of integrated electrodes based on electrospun fibers using the drop-casting method: (**a**) adapted with permission from Ref. [147]. (**b**) adapted with permission from Ref. [148]. (**c**) adapted with permission from Ref. [149]. (**d**) adapted with permission from Ref. [150]. (**e**) adapted with permission from Ref. [151]. (**f**) adapted with permission from Ref. [152].

A critical stage in the process is the thermal treatment (calcination), which removes the polymer matrix and converts the precursors into metal oxides. The calcination parameters, such as temperature, heating rate, and duration, directly affect the crystallinity and grain size, which in turn determine the gas-sensing properties of the resulting fibers [111].

There are several methods for forming electrodes based on electrospun nanofibers. One approach involves depositing the fibers onto integrated electrodes followed by calcination, which ensures strong adhesion between the components and enhances the sensor's performance [147–154].

Another method involves the pre-coating of fibers onto ceramic tubular electrodes, which enhances adhesion and increases the number of active centers for interaction with the gas environment (see Figure 8). This approach improves the sensor's sensitivity and simplifies the sensor assembly process [155–158].

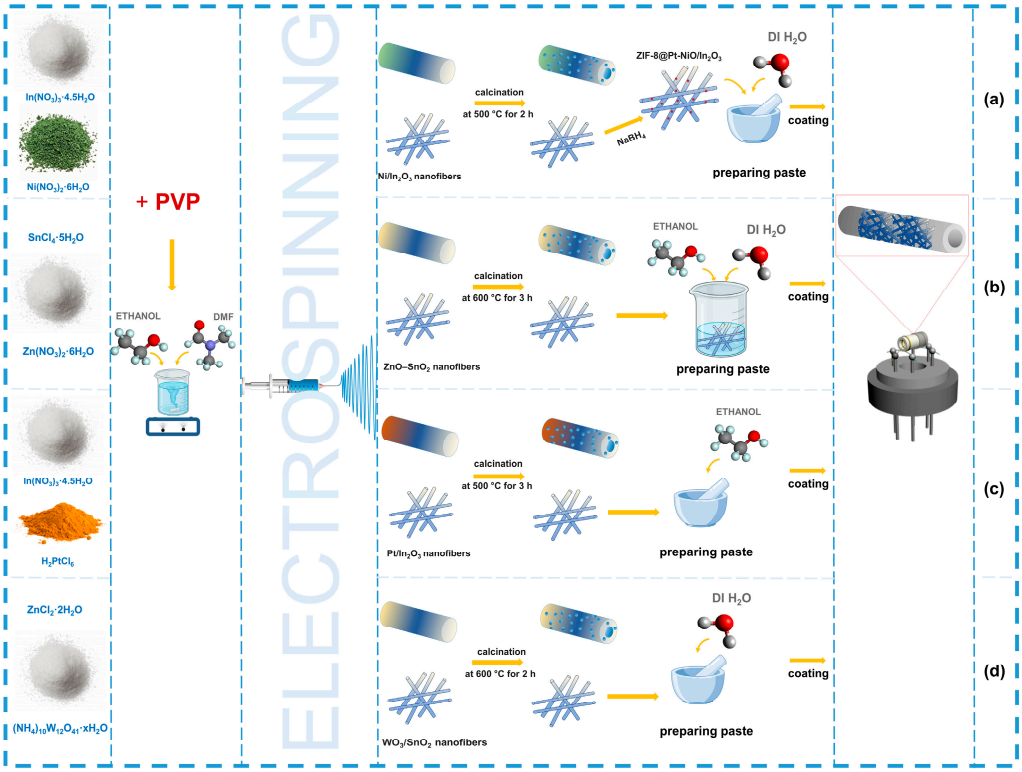

Figure 8. Fabrication of tubular electrodes based on electrospun fibers using coatings: (**a**) adapted with permission from Ref. [155]. (**b**) adapted with permission from Ref. [156]. (**c**) adapted with permission from Ref. [157]. (**d**) adapted with permission from Ref. [158].

In some studies, electrodes are formed directly during the electrospinning process. This method allows for optimized adhesion, precise control over the coating thickness, and improved electrode performance (see Figure 9) [159–161].

Therefore, the successful development of chemoresistive sensors based on electrospun nanofibers requires a comprehensive approach that includes material selection, optimization of electrospinning and thermal treatment parameters, and the development of effective methods for integrating fibers with electrodes. Careful management of these parameters is essential to achieve high sensitivity, stability, and selectivity in the sensors.

Moreover, achieving these characteristics necessitates consideration of the analyte's nature and its interaction with the gas-sensitive material's surface. The sensor's effectiveness is influenced not only by the fiber morphology but also by the reducing and oxidizing properties of the analytes, which can affect the interaction mechanisms with the sensitive material. These factors directly impact the accuracy and reliability of measurements, underscoring the importance of a holistic approach in the development and optimization of gas-sensitive sensors.

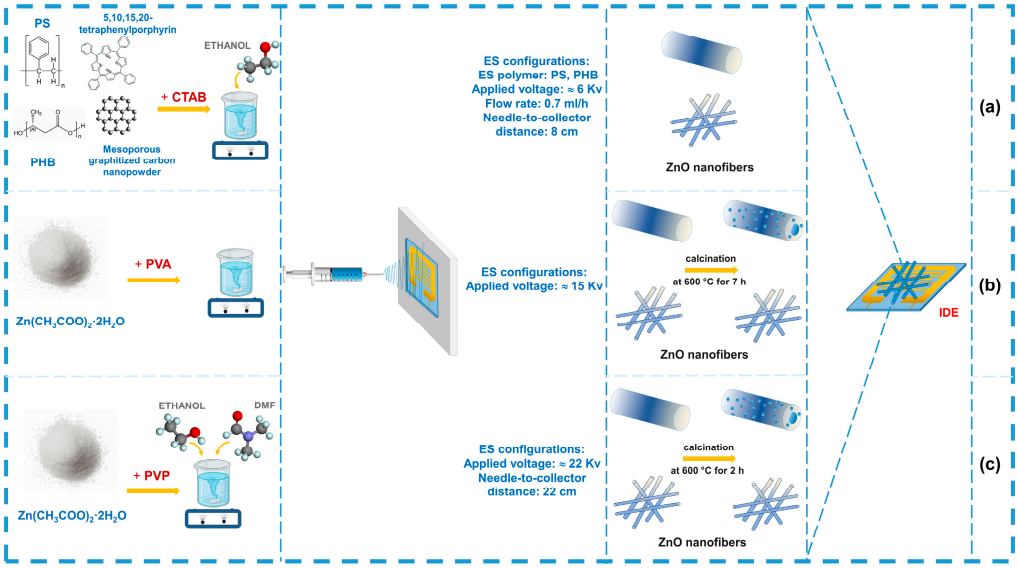

Figure 9. Fabrication of electrodes on the collector: (**a**) adapted with permission from Ref. [159]. (**b**) adapted with permission from Ref. [160]. (**c**) adapted with permission from Ref. [161].

4.1. Gas-Sensitive Characteristics to Reducing Gases

Detecting reducing gases such as acetone, hydrogen, and ammonia is critically important for safety, environmental protection, and health [162–164]. These gases are widely used in industry and agriculture, but their leaks can lead to toxic effects, explosions, and deteriorated air quality [165]. For example, hydrogen, while a promising fuel, is highly flammable if leaked, and ammonia is toxic at high concentrations [166,167]. Early detection of such gases in environmental monitoring and industrial safety allows for timely responses to potential threats, helps prevent accidents, and minimizes harmful impacts on the environment and human health [168].

One promising research direction is the use of composite nanofibers based on metal oxides. The shape and structure of these fibers significantly influence their gas-sensing properties, as demonstrated by numerous studies on the detection of reducing gases.

An effective approach to enhance sensor performance is the use of nanofibers doped with nanostructures. For example, research [169] has shown the effectiveness of Fe_2O_3 nanotubes doped with terbium (Tb) for acetone detection. These nanofibers, produced via electrospinning and calcined at 550 °C, exhibited a response of 53.2 at a concentration of 50 ppm acetone and 170 °C, which is 13 times greater than the sensitivity of pure Fe_2O_3 nanotubes. The doping with terbium further increases the concentration of oxygen vacancies, improving interaction with gas molecules. The unique morphology of the hollow-structured nanotubes explains the high sensor response (53.2 at 50 ppm acetone) and low detection limit (200 ppb).

The morphology of nanofibers is also critically important for the stability and sensitivity of composite-based sensors. For example, composite fibers of CuO/ZnO synthesized via electrospinning (see Figure 10a–c) exhibit a porous and scaly structure, which contributes to high sensitivity and stability towards hydrogen sulfide (H_2S) [170].

Modifying the morphology of fibers with noble metals such as gold and palladium also significantly enhances their sensitivity. For example, In_2O_3 nanofibers doped with 2 at.% Au and 2 at.% Pd exhibit a marked improvement in response to CO due to the increased conductivity provided by the noble metals (see Figure 10d–f) [171]. This also highlights the importance of fiber morphology in ensuring sensor sensitivity, as it affects the interaction process between the gas and active surfaces.

Despite identical synthesis conditions, such as applied voltage and the distance between the needle and the collector during electrospinning, the fiber morphology can vary significantly. For instance, composite fibers of PANI/hollow Carbon#In_2O_3 exhibit a pro-

nounced surface roughness and a hollow structure (see Figure 10g–i), which enhance the binding of ammonia molecules [172]. These fibers demonstrate stability at low gas concentrations (1 ppm), highlighting the crucial role of morphology control in ensuring both the stability and sensitivity of sensors.

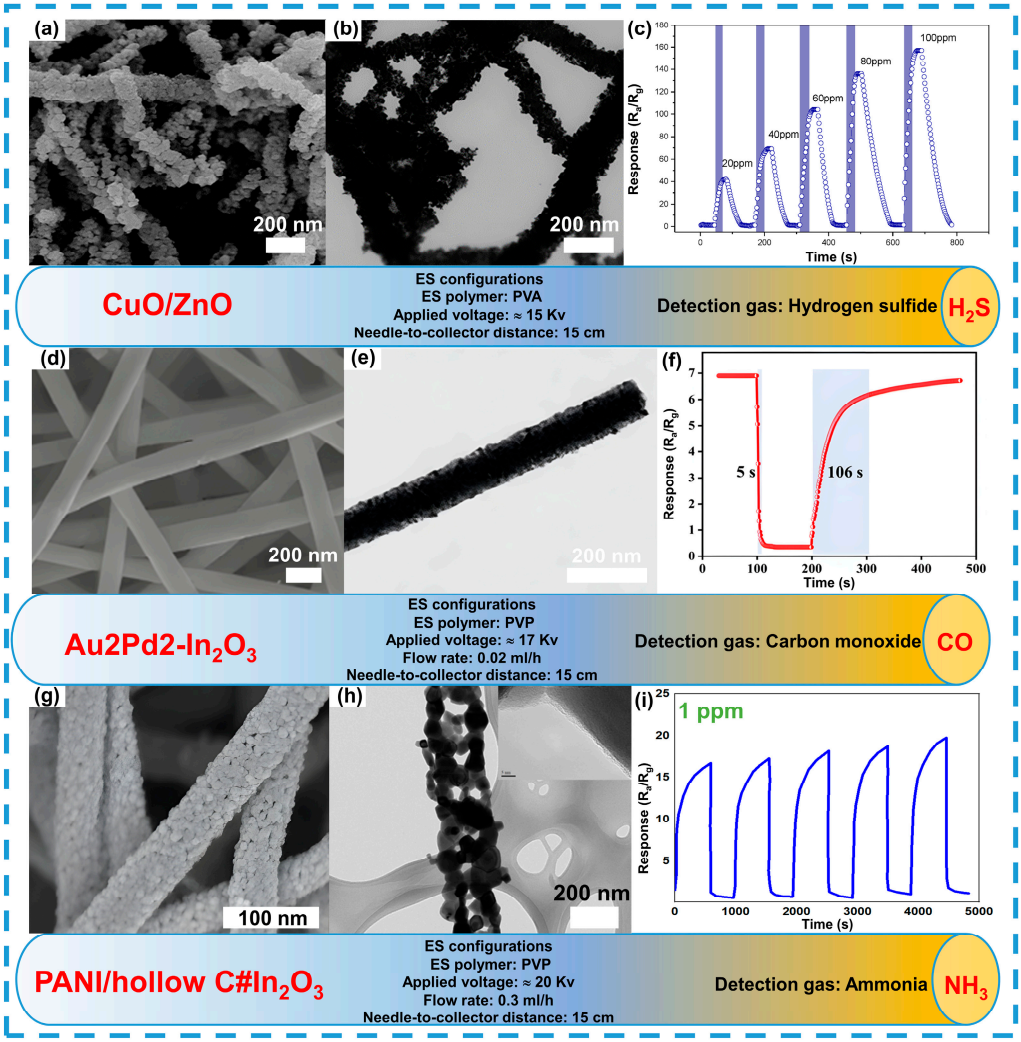

Figure 10. Morphology and structure of composite fibers as an example of reductive gas detection. Detection to H_2S (**a**–**c**), reprinted with permission from Ref. [170]. CO (**d**–**f**), reprinted with permission from Ref. [171]. NH_3 (**g**–**i**), reprinted with permission from Ref. [172].

Another important area is the development of nanocomposites based on rGO, which enhances the sensitivity and selectivity of sensors. In a study [173], NiO nanofibers wrapped with rGO were synthesized for ammonia detection. This nanocomposite is characterized by high conductivity and increased specific surface area, which improves sensor sensitivity and accelerates response time. NiO creates active centers for NH_3 adsorption, increasing material conductivity through interaction with nickel vacancies. The rGO-NiO sensor demonstrated high sensitivity to NH_3 at a concentration of 50 ppm, with a response time of 32 s and a recovery time of 38 s. The high repeatability of the response confirms the sensor's stable performance over extended periods.

The use of carbon nanomaterials, produced via electrospinning, not only provides a high specific surface area but also imparts mechanical flexibility to the sensors, which is relevant for flexible electronics. In a study by Xing Fan and colleagues [174], a flexible sensor based on electrospun carbon nanofibers (CNF) decorated with ZnO nanoparticles (ZnO@CNF) was developed for ammonia detection. The electrospun carbon nanofibers,

obtained through electrospinning, carbonization, and pre-oxidation, serve as a flexible substrate for the even distribution of ZnO nanoparticles, ensuring stable sensor performance under mechanical deformation. The formation of a p-n heterojunction between ZnO and CNF provides enhanced properties compared to the individual components. At room temperature, ammonia reacts with oxygen ions on the ZnO surface, leading to the release of electrons and a decrease in sensor resistance. The sensor operates effectively at 23 °C, unlike higher temperatures required for sensors based on pure ZnO. Under high humidity conditions, the sensor also responds to the presence of water, leading to the formation of hydronium ions (H_3O^+) and an increased response. The sensor exhibits short response and recovery times—5 and 18 s, respectively—and maintains its properties after multiple mechanical bends, making it reliable for use in flexible devices.

The use of nanowires and nanorods also enhances the gas-sensing properties of sensors by increasing the surface-to-volume ratio. In a study by Cai Z. and Park S. [175], SnO_2 nanofibers doped with palladium and In_2O_3 were synthesized for hydrogen detection. Palladium nanoparticles facilitate the formation of Schottky barriers and catalytic activation, significantly improving hydrogen sensitivity. Doping with In_2O_3 resulted in a 24-fold increase in sensor sensitivity compared to materials containing only palladium.

Thus, employing nanoscale structures, such as nanotubes, nanofibers, nanorods, and nanocomposites, significantly expands the capabilities of gas sensors for detecting reducing gases. The application of these nanomaterials notably enhances key sensor parameters, including sensitivity, selectivity, and operating temperature. Furthermore, these sensors demonstrate high stability and durability, maintaining their performance under repeated mechanical deformations and prolonged use. This makes them particularly promising for applications in flexible electronics and environmental monitoring systems.

The table below provides a comparative analysis of sensors for detecting various reducing gases, detailing materials, electrospinning parameters, target gases, response and recovery times, operating temperatures, and detection limits, highlighting the diversity of approaches and their adaptation to various practical requirements. See Table 2.

Table 2. Comparison of electrospun-fiber-based sensors for detecting reducing gases.

Materials	ES Parameters			Target Gas	Response Time	Recovery Time	Operating T°C	Selectivity	Detection Range, ppm	Sensitive Concentration, ppm	Ref.
	Flow Rate, mL/h	Voltage, kv	Needle-to-Collector Distance, cm								
SnO_2-loaded ZnO	0.01	15	20	H_2	–	–	300	H_2, CO, NO_2	0.05–5	5	[150]
ZnO	–	22	22	H_2	–	–	210–330	H_2	20–100	100	[160]
PANI/PEO/ZnO	1.3	25	20	NH_3	245	153	RT	H_2, H_2S	250	250	[176]
p-NiO-loaded n-ZnO	0.02	15	20	H_2	–	–	200	H_2, H_2S, CO, C_6H_6	0.1–10	10	[177]
PVA/PEDOT:PSS	10 m s^{-1}	20	15	NH_3	10	–	RT	NH_3	50	50	[178]
ZnO	0.56	12	15	H_2S	14	49	180	H_2S, VOCs, NH_3	50	50	[179]
PPy-PAN	0.8	10	20	NH_3	1	60	RT	VOCs	250–2000	2000	[180]
NiO/SnO_2	1	12	15	H_2	12	5	195	H_2	25–100	25	[181]
CuO-SnO_2	0.4	8	12	H_2S	284	539	150	NO, CO, CH_4, SO_2, C_2H_5OH	1–10	10	[182]
CFs@NiNPs–PtNPs	1	25	21	H_2	24	89	RT	H2, NH_3	10,000–40,000	1000	[183]
SnO_2	–	17	–	H_2S	15	230	350	H_2S, CO, H_2, SO_2, NH_3	0.1–1	1	[184]
Cu/CuO@ZnO	1.2	20	15	CO	–	–	400	–	–	100	[185]
Co_3O_4	0.707	20	10	CO	14	36	100	CO, NO_2, H_2, CH_4, NH_3	5–40	5	[186]

Thus, electrospun nanofibers are promising materials for the detection of reducing gases due to their high sensitivity and stability.

4.2. Gas-Sensitive Characteristics to Oxidizing Gases

Detecting oxidizing gases such as nitrogen dioxide (NO_2), ozone (O_3), and sulfur dioxide (SO_2) is crucial for mitigating environmental and industrial risks [187]. These gases can have serious health impacts, contribute to environmental pollution, and cause damage to industrial equipment. For instance, NO_2 and SO_2 are major pollutants that contribute to acid rain formation and deteriorate air quality in urban areas [188,189]. Ozone, on the other hand, poses health risks when present in high concentrations in the lower atmosphere. Reliable and sensitive sensors capable of detecting even trace concentrations of these gases are essential for environmental protection, emission monitoring, and preventing industrial accidents [190].

A promising research direction involves the use of composite nanofibers based on metal oxides [39]. The morphology of these fibers plays a crucial role in their gas-sensing characteristics, as demonstrated by numerous studies.

For example, in study [143], nanofibers made from a mixture of CuO and Fe_2O_3, produced via electrospinning, showed an enhanced response to NO_2. Nanofibers with a $0.5CuO\text{-}0.5Fe_2O_3$ ratio were particularly effective, forming a binary oxide $CuFe_2O_4$ that creates heterojunctions between oxides, thereby enhancing sensor sensitivity. The morphology of these fibers, developed during the electrospinning process, improves the contact between active surfaces and gas molecules, significantly affecting their gas-sensing properties. The spinning time also plays a crucial role in shaping the fiber structure, which directly impacts response characteristics.

Another example is study [191], which investigates porous $NiFe_2O_4$ nanofibers with nanocrystallites, showing high sensitivity to H_2S and NO_2. The porous structure of these fibers increases surface area and enhances interaction with gases, improving sensor response. In this case, electrospinning conditions such as voltage directly influence morphology and, consequently, sensor sensitivity to different gases.

Particular attention is given to sensors based on materials that utilize optical excitation through localized surface plasmon resonance. For instance, Au/SnO_2 nanofibers synthesized via electrospinning exhibit enhanced gas sensitivity under UV irradiation due to the gold's surface plasmon effect (see Figure 11a–c) [192]. The fine morphology of the fibers improves photon transfer and increases the number of active centers for gas molecule interaction.

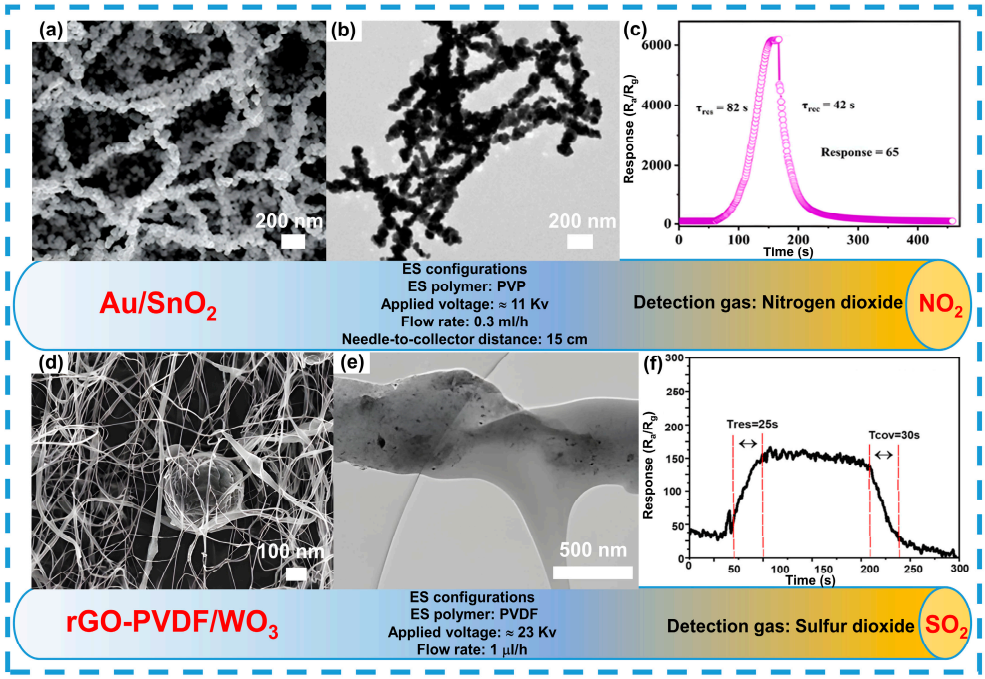

Figure 11. Morphology and structure of composite fibers as an example of oxidizing gas detection. Detection to NO_2 (**a**–**c**), reprinted with permission from Ref. [192]. SO_2 (**d**–**f**), reprinted with permission from Ref. [193].

It is also important to note that incorporating reduced graphene oxides into composite fibers improves the sensor recovery time, which is related to increased overall porosity and conductivity of the fibers. Specifically, rGO-PVDF/WO_3 nanofibers demonstrate high sensitivity to SO_2 due to their porous structure and enhanced surface area (see Figure 11d–f) [193]. See Table 3.

Table 3. Comparison of electrospun-fiber-based sensors for detecting oxidizing gases.

Materials	ES Parameters			Target Gas	Response Time	Recovery Time	Operating T°C	Selectivity	Detection Range, ppm	Sensitive Concentration, ppm	Ref.
	Flow Rate, mL/h	Voltage, kv	Needle-to-Collector Distance, cm								
ZnO/Bi_2O_3 ZnO/In_2O_3	0.8–1	20	18	NO_2	5–7	–	200	NO_2	0.5–3	0.5	[194]
SFRGO	0.5	20	15	NO_2	–	–	RT	NO_2, VOCs	0.01–20	20	[195]
Au-PANI/ZnO	0.5	16	14	NO_2	–	–	300	H_2, NO_2, CO, NH_3	10–50	50	[196]
WO_3	0.5	14.5	15	NO_2	11	26	200	NO_2, VOCs	0.2–50	1	[197]
PdOx@SnO_x	0.3	1.2	–	NO_2	–	–	325	NO_2, CO, NH_3	0.0625–0.25	0.25	[198]
SnO_2/ZnO	–	20	20	NO_2	126	–	RT	NO_2, SO_2, CO, NH_3, VOCs	0.1–2	0.5	[199]
PANI/g-C_3H_8/PVDF	0.5	15	17	NO_2	–	–	RT	NO_2, NH_3, VOCs	8–108	108	[200]
WO_3	0.06	20	15	NO_2	15 min	0.8 min	150	NO_2, H_2, CO	2–25	25	[201]
rGO-PVDF/WO_3	0.001	23	10	SO_2	25	30	200	SO_2, NH_3, CO_2, VOCs	5–80	80	[193]
MoS_2/SnO_2	–	17	13	SO_2	–	–	150	SO_2, CO, H_2, NH_3	1–10	10	[202]
Zr-MOF	–	–	–	SO_2	185	–	RT	SO_2	1–150	50	[203]

Thus, the morphology of nanofibers plays a crucial role in achieving high gas-sensing performance in sensors. The electrospinning method offers unique opportunities to tailor this morphology, allowing for customization of sensors for specific gas-detection tasks. Comparative analysis of various studies demonstrates that the fiber structure and electrospinning conditions significantly influence sensor response, sensitivity, and selectivity. This makes fiber morphology a critical factor in the development of advanced gas analyzers.

4.3. Gas-Sensitive Characteristics to Volatile Organic Compounds (VOCs)

The detection of volatile organic compounds plays a crucial role in air quality control and assessing their impact on human health and the environment [204]. VOCs, such as benzene, toluene, and xylene, are widely used in industry and consumer products, but their emissions into the atmosphere can lead to smog formation, greenhouse gas effects, and adverse health impacts, including respiratory diseases and cancer [205]. VOCs readily evaporate at room temperature, making them challenging to detect without highly sensitive sensors. Monitoring VOCs is increasingly relevant in the context of growing urbanization and rising industrial emissions. Modern gas sensors with high selectivity and low detection limits can detect even trace concentrations of VOCs, which is essential for risk assessment and compliance with environmental and health regulations [206,207].

Electrospinning is a method for producing ultrathin fibers with a high specific surface area and controlled structure, which is critical for achieving high sensitivity and selectivity in gas sensors.

Furthermore, increasing the number of oxygen vacancies can be achieved by using MOFs to create porous structures that retain the morphological properties of precursors after thermal treatment. This contributes to an increase in active oxygen content and improved gas-sensing properties. Recent studies have proposed using polycrystalline ZIF-8 to enhance adsorption characteristics, which allows for the creation of more oxygen

vacancies and improved sensitivity to ammonia and formaldehyde. Nanofibers of Pt/ZnO-In_2O_3 derived from Pt/ZIF-8 provide a 2.7-fold greater response to formaldehyde compared to pure In_2O_3, with fast response and recovery times (see Figure 12a–c) [208].

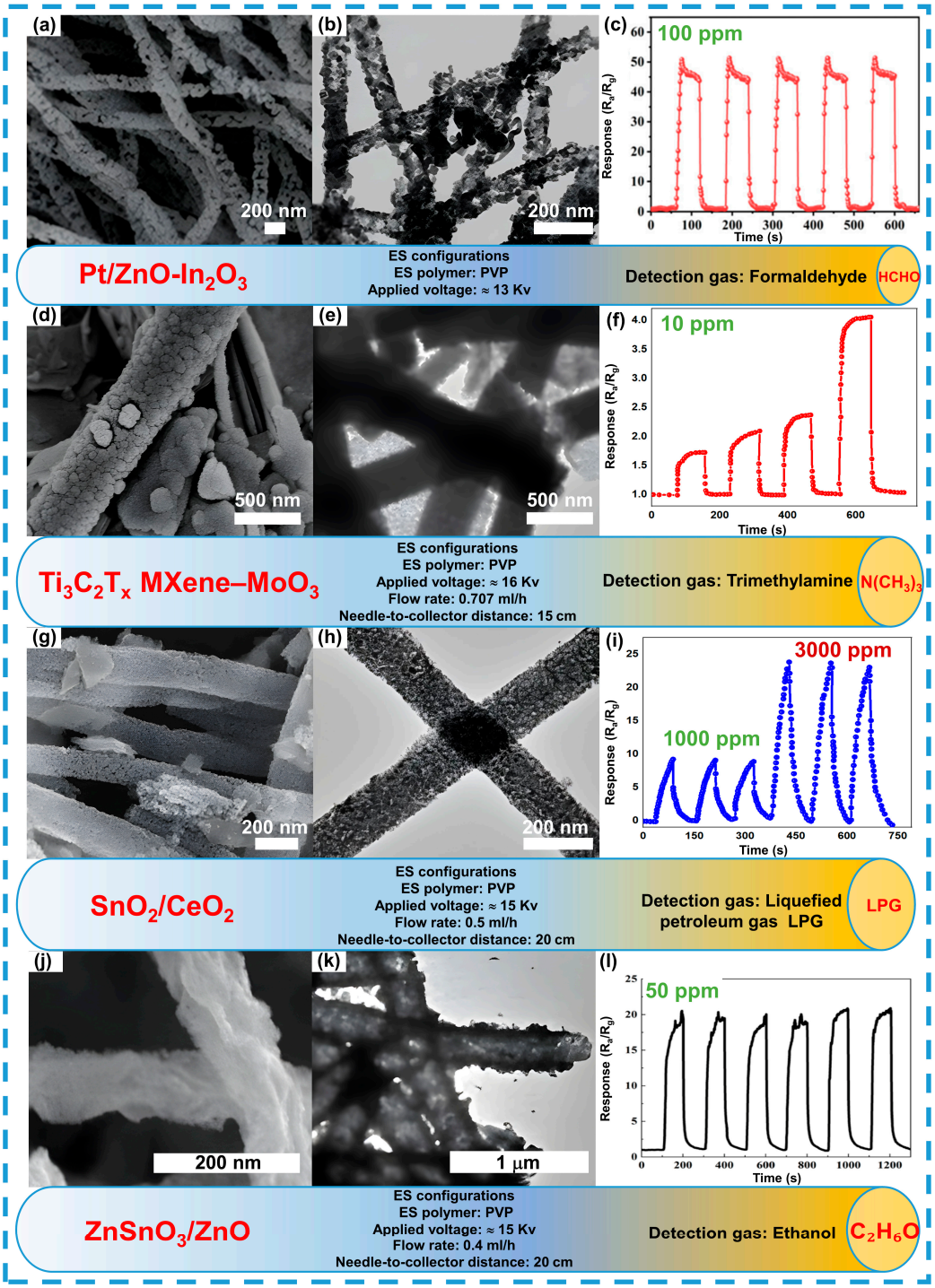

Figure 12. Morphology and structure of composite fibers as an example of VOCS detection. Detection to HCHO (**a**–**c**), reprinted with permission from Ref. [208]. $N(CH_3)_3$ (**d**–**f**), reprinted with permission from Ref. [209]. LPG (**g**–**i**), reprinted with permission from Ref. [210]. Ethanol (**j**–**l**), reprinted with permission from Ref. [211].

The interaction of two-dimensional MXene materials with one-dimensional metal oxide semiconductors also contributes to improved sensor characteristics. Nanofibers of

MoO_3 and layered Ti_3C_2Tx MXene, produced using electrospinning and chemical etching, demonstrate outstanding results in detecting trimethylamine. The Ti_3C_2Tx MXene–MoO_3 composite material shows high response and rapid response-recovery times due to its significant specific surface area, active centers, and p-n heterojunctions (see Figure 12d–f) [209].

Nanofibers of tin dioxide (SnO_2) and cerium dioxide (CeO_2) nanoparticles, produced using electrospinning and hydrothermal synthesis, show significant improvement in sensitivity for detecting liquefied petroleum gas. The SnO_2/CeO_2 composite sensor exhibits enhanced sensitivity and moisture resistance compared to pure SnO_2, which can be attributed to an increased number of oxygen vacancies and the formation of a heterostructure (see Figure 12g–i) [210].

The addition of various components to the composite structure significantly influences the morphology, altering the fiber surface and their gas-sensing properties. For instance, a study produced tri-metallic composite fibers of $ZnSnO_3/ZnO$, which, with their hollow and rough structure (see Figure 12j–l), show stability in ethanol detection [211].

Additionally, it is possible to create composite materials that are entirely metal-free. In one study, fibers made from polyacrylonitrile/polyaniline (PAN/PANI) via electrospinning exhibited outstanding performance in detecting trimethylamine, achieving detection limits below 6 ppb and providing excellent repeatability [212]. These results affirm the effectiveness of using nanofibers for creating highly sensitive and stable sensors for volatile organic compounds. The comparative analysis table of various sensors highlights their advantages and limitations, making the use of electrospun nanofibers a promising approach for enhancing the monitoring and control of volatile organic compound concentrations in various environments. These fibers possess unique properties, such as high specific surface area and a high density of active centers, making them particularly suitable for detecting low concentrations of various VOCs.

The table provides a comparative analysis of different sensors for detecting volatile organic compounds, including their key parameters and characteristics. It lists sensor materials, electrospinning parameters (flow rate, voltage, and distance between the needle and collector), target gases, response and recovery times, operating temperature, selectivity, detection range, and sensitivity concentration for each material. For instance, a Pt-SnO_2-based sensor demonstrates high sensitivity to acetone with a detection range from 0.1 to 20 ppm and a response time of 13 s. Similarly, a Rh-SnO_2-based sensor is also designed for acetone detection but features a broader detection range (90–200 ppm) and a slower response time (2 s). See Table 4.

Table 4. Comparison of electrospun-fiber-based sensors for detecting VOCs.

Materials	ES Parameters			Target Gas	Response Time	Recovery Time	Operating T°C	Selectivity	Detection Range, ppm	Sensitive Concentration, ppm	Ref.
	Flow Rate, mL/h	Voltage, kv	Needle-to- Collector Distance, cm								
Pt-SnO_2	0.003	15	15	Acetone	13	24	150	VOCs	0.1–20	2	[213]
Rh-SnO_2	0.3	13	13	Acetone	2	64	200	VOCs	90–200	50	[110]
SnO_2/ZnO	–	20	15	Acetone	12 s	27 s	350	VOCs	1–100	5	[214]
Pt-SnO_2	0.03	15	20	C_7H_8	–	–	300	C_6H_6, C_7H_8, CO	1–10	10	[215]
ZnO	–	18	20	Acetone	40	30	260	VOCs		50	[216]
Co–CeO_2@SnO_2	0.3	16	10	C_5H_8	5 s	514 s	350	VOCs	0.1–5	5	[217]
MoO_3-WO_3	1	20	15	Acetone	–	–	375	VOCs, $NH_3 \cdot H_2O$	20–1000	100	[218]
PANI/P_3TI/PMMA	0.6	20	10	n-Butanol	10	–	RT	n-Butanol, CB, DMF, n-Propanol, Toluene	100–2000	100	[219]
CuO	0.3	–	12	VOCs	–	–	RT	H_2, Ethanol, LPG	50–350	350	[220]
Pd-CeO_2	0.5	15	15	Methanol	1	5	200	H_2, NH_3, CO, VOCs	5–2000	100	[221]
Au-SnO_2	0.008	11	5	Tetrahydrocannabinol	–	–	350	Tetrahydrocannabinol, Methanol	200–1000	1000	[222]
Co_3O_4	0.016	7	7	Methanol	15	26	350	VOCs	21–2094	4–2094	[223]
EPS/rGO	1	15	20	Ethanol	110	20	RT	Ethanol, acetone, toluene	10–80	10	[224]
Pd@Co_3O_4-ZnO	–	10	10	Ethanol	6	12	240	Ethanol, acetone, isopropanol	1–2000	200	[225]

Other sensors, such as MoO_3-WO_3 and Pd@Co_3O_4-ZnO, exhibit significant recovery times and wide detection ranges, making them suitable for various applications and types of VOCs. Comparing these sensors highlights their advantages and limitations to VOC monitoring. Therefore, the use of electrospun nanofibers for detecting volatile organic compounds represents a promising direction that can significantly enhance the monitoring and control of VOC concentrations in diverse environments.

5. Challenges and Future Directions

The increasing emissions of toxic gases are driving the demand for modern, cost-effective devices for their detection and monitoring. These gases pose a significant threat to human health, making accurate and continuous monitoring of their concentrations essential. Gas sensors, with their relatively low cost and ease of use, remain ideal for environmental monitoring, though their selectivity and durability still require further optimization to meet the needs of contemporary industries. In medicine, gas sensors are used for diagnosing diseases based on breath analysis. For instance, the detection of biomarkers like ammonia serves as an indicator of liver and kidney diseases, opening new possibilities for rapid, non-invasive diagnostics. This method could complement traditional blood and urine tests, providing a convenient and safe tool for health screening and monitoring [226]. Moreover, chemoresistive sensors show potential for food quality control, as they can detect volatile compounds that indicate spoilage, enabling automated monitoring systems that can be integrated into household devices [227].

Research into new synthesis methods and the effects of dopants on the gas-sensing properties of materials remains key to the development of multisensor systems. Despite the promising sensitivity of heterojunctions to NO_2 under high humidity, the precise mechanisms of their operation are not yet fully understood. One of the main challenges for sensors in breath analysis is the high relative humidity, which can reach nearly 100%, significantly altering gas-sensing mechanisms. Under low humidity, sensors typically operate based on oxygen adsorption, but at high humidity, the mechanism shifts to physical water adsorption through the Grotthuss mechanism. This complicates the development of sensors that can effectively function under conditions similar to exhaled breath.

On the other hand, reducing energy consumption remains another critical challenge, as the high operating temperatures of metal oxide semiconductor sensors (100–450 °C) [228] present significant issues for practical use. These sensors require high temperatures, leading to reduced long-term stability, increased production costs, and higher energy consumption. These limitations make them less suitable for portable devices, where low power consumption and compact size are crucial. Recent studies have proposed various solutions, including the use of low-power LEDs [229], functionalization with noble metals [230], hybrid materials [231], self-heating modes, and integration with MEMS platforms [232]. However, despite these advancements, doping SMOx materials with transition metals and rare earth elements remains a promising direction for further improving sensor performance. This allows for the optimization of electrical and surface properties, thereby enhancing gas sensitivity and device stability. In advanced applications, semiconductors doped with rare-earth oxides are recognized as among the most suitable materials due to their enhanced selectivity and durability [233]. For example, studies have shown that doping metal oxides with praseodymium and europium improves the humidity resistance of sensors by neutralizing the effects of hydroxyl groups and restoring sensitivity to NO_2 [234]. This approach could be the foundation for developing sensors that are independent of humidity levels.

At the same time, unresolved issues of sensor reproducibility, scalability, and sensitivity remain. Although commercial electrochemical sensors for NO_2 detection are already available, they still struggle to reach ppb-level sensitivity [235]. Meanwhile, 1D carbon materials exhibit limited sensitivity to specific gases without surface modification. Functionalization or doping of materials such as SMOx and transition metal dichalcogenides can enhance their gas-sensing properties and address issues of durability and aggregation

in carbon nanotubes and nanofibers. In this context, the electrospinning method can be a crucial tool. Electrospinning allows for the creation of nanofibers with a high surface area and unique morphology, which can significantly improve the sensitivity and selectivity of sensors by increasing the number of active centers for gas interaction.

However, sensor selectivity toward various gases remains a major challenge. Modern materials often show high sensitivity to one gas but low sensitivity to others. Detecting gases with similar physicochemical properties is even more difficult. Furthermore, the need to develop individual sensors for each specific gas makes the process labor-intensive and expensive, demanding further innovation [236].

In a recent study, researchers demonstrated the potential of using heterostructures based on 2D metal sulfides and oxides to enhance gas sensitivity due to the unique electronic properties at the interface. They showed that heterostructures of SnS and SnS_2-SnO_2 in the form of vertically oriented 1D nanostructures exhibited improved sensitivity to NO_2 at high humidity (90% RH), with a theoretical detection limit of 1.67 ppt [237]. The moisture resistance of tin sulfides maintained active centers for gas interaction, ensuring high sensitivity.

The future of gas sensors lies in their integration with other sensing technologies, which will allow for increased sensitivity and the creation of more complex gas monitoring systems. The electrospinning method represents a promising direction, enabling the creation of new structures with unique properties, enhancing sensor sensitivity and selectivity. Success in gas sensor development will require an interdisciplinary approach, bringing together expertise in materials science, chemistry, and engineering. Through collaboration, it will be possible to integrate new materials and synthesis methods, leading to the creation of more efficient sensor systems for a wide range of applications [238].

6. Conclusions

This review article highlights the critical role of gas sensors, particularly those based on electrospun nanofibers, in ensuring safety and air quality control across various fields—from industry to medicine. The electrospinning technique enables the formation of nanofibers with unique morphologies characterized by high surface area and porous structures. These features significantly enhance key gas-sensing properties of sensors, such as sensitivity, selectivity, and response time.

Despite substantial advancements in nanomaterials and technologies, nanofiber-based sensors face significant challenges, including limited selectivity for specific gases and difficulties in scaling up for mass production. Promising research directions include optimizing fiber morphology, incorporating functional materials, and developing advanced post-annealing techniques such as surface modification or doping with active elements. These approaches are expected to improve the selectivity and stability of sensors, unlocking new possibilities for their effective application in real-world conditions.

Thus, focusing on the precise tuning of electrospun fiber morphology and its impact on gas-sensing properties is a key aspect of advancing gas monitoring technologies. It is anticipated that a detailed analysis of new materials and methods will overcome existing limitations, significantly enhancing the performance of gas sensors and broadening their application across various industries.

Author Contributions: A.I.: Investigation, Methodology, Visualization, Writing—Review and Editing; G.S.: Supervision, Formal analysis, Writing—Review and Editing, Funding acquisition; B.K.: Project administration, Investigation, Visualization, Writing—Review and Editing; A.K.: Conceptualization, Data curation, Writing—review and editing; R.K.: Writing—original draft preparation, Resources; L.F.V.: Software, Writing—original draft preparation; Z.M.: Formal analysis, Data curation. All authors have read and agreed to the published version of the manuscript.

Funding: This work was funded by Ministry of Science and Higher Education of the Republic of Kazakhstan, grant number AP19679885.

Institutional Review Board Statement: Not applicable. The authors declare that the manuscript does not involve or relate to animals, human subjects, human tissues, or plants.

Informed Consent Statement: Not applicable.

Data Availability Statement: Data are contained within the article.

Conflicts of Interest: The authors declare that they have no competing interests that could influence the work presented in this manuscript.

References

1. Korotcenkov, G. II–VI Semiconductor-Based Conductometric Gas Sensors: Is There a Future for These Sensors? *Sensors* **2024**, *24*, 3861. [CrossRef] [PubMed]
2. Wales, D.J.; Grand, J.; Ting, V.P.; Burke, R.D.; Edler, K.J.; Bowen, C.R.; Mintova, S.; Burrows, A.D. Gas Sensing Using Porous Materials for Automotive Applications. *Chem. Soc. Rev.* **2015**, *44*, 4290–4321. [CrossRef]
3. Rajagukguk, J.; Pratiwi, R.A.; Kaewnuam, E. Emission Gas Detector (EGD) for Detecting Vehicle Exhaust Based on Combined Gas Sensors. *J. Phys. Conf. Ser.* **2018**, *1120*, 012020. [CrossRef]
4. Rodríguez-Aguilar, M.; Díaz De León-Martínez, L.; Gorocica-Rosete, P.; Pérez-Padilla, R.; Domínguez-Reyes, C.A.; Tenorio-Torres, J.A.; Ornelas-Rebolledo, O.; Mehta, G.; Zamora-Mendoza, B.N.; Flores-Ramírez, R. Application of Chemoresistive Gas Sensors and Chemometric Analysis to Differentiate the Fingerprints of Global Volatile Organic Compounds from Diseases. Preliminary Results of COPD, Lung Cancer and Breast Cancer. *Clin. Chim. Acta* **2021**, *518*, 83–92. [CrossRef]
5. Hong, H.S.; Hoang, T.V.; Huong, N.T.; Nam, N.H.; Thinh, D.D.; Hue, N.T.; Thuan, N.D. Ultra-Low Detection Limit Chemoresistive NO_2 Gas Sensor Using Single Transferred MoS_2 Flake: An Advanced Nanofabrication. *RSC Adv.* **2022**, *12*, 33403–33408. [CrossRef]
6. Shinde, P.V.; Xia, Q.X.; Ghule, B.G.; Shinde, N.M.; Seonghee, J.; Kim, K.H.; Mane, R.S. Hydrothermally Grown α-MnO_2 Interlocked Mesoporous Micro-Cubes of Several Nanocrystals as Selective and Sensitive Nitrogen Dioxide Chemoresistive Gas Sensors. *Appl. Surf. Sci.* **2018**, *442*, 178–184. [CrossRef]
7. Garg, G.; Garg, N.; Deep, A.; Soni, D. Zr-MOF and PEDOT:PSS Composite Sensor for Chemoresistive Sensing of Toluene at Room Temperature. *J. Alloys Compd.* **2023**, *956*, 170309. [CrossRef]
8. Nadekar, B.; Khollam, Y.B.; Shaikh, S.F.; Wavhal, D.; Varshney, P.; Pandit, B.; More, P.S. Enhanced Ammonia/Amines Sensitivity at Room Temperature Using Plasma Polymerized Polyvinyl Acetate-Reduced Graphene Oxide Composite Film Sensors. *Surf. Interfaces* **2023**, *42*, 103453. [CrossRef]
9. Lin, M.; Huang, Y.; Liu, Y.; Liu, N.; Lei, Z.; Huang, C.; Cao, J.; Ouyang, X.; Zhou, Y. A Durable Gas Sensor Based on $AgVO_3/TiO_2$ Nanoheterostructures to Ethanol Gas. *J. Alloys Compd.* **2023**, *961*, 171103. [CrossRef]
10. Zhang, G.; Li, C.; Cheng, F.; Chen, J. $ZnFe_2O_4$ Tubes: Synthesis and Application to Gas Sensors with High Sensitivity and Low-Energy Consumption. *Sens. Actuators B Chem.* **2007**, *120*, 403–410. [CrossRef]
11. Mustaffa, S.N.A.; Ariffin, N.A.; Khalaf, A.L.; Yaacob, M.H.; Tamchek, N.; Paiman, S.; Sagadevan, S. Sensing Mechanism of an Optimized Room Temperature Optical Hydrogen Gas Sensor Made of Zinc Oxide Thin Films. *J. Mater. Res. Technol.* **2020**, *9*, 10624–10634. [CrossRef]
12. Gong, L.; Zhang, Y.; Liu, R.; Liu, Z.; Jin, S.; Zhang, L.; Zhao, T.; Fa, H.; Yin, W. A Portable Electrochemical Room-Temperature Sensor Based on Flower-like Structure UIO-66-NH_2@MoS_2 Composite for Ammonia Detection. *Sens. Actuators B Chem.* **2024**, *413*, 135868. [CrossRef]
13. Mirzaei, A.; Sun, G.-J.; Lee, J.K.; Lee, C.; Choi, S.; Kim, H.W. Hydrogen Sensing Properties and Mechanism of NiO-Nb_2O_5 Composite Nanoparticle-Based Electrical Gas Sensors. *Ceram. Int.* **2017**, *43*, 5247–5254. [CrossRef]
14. Huang, S.; Zhao, X.; Hao, C.; Ma, Z.; Wang, H.; Zhang, A.; Zhang, W.; Li, L.; Zhang, W. Multifunctional PVDF/CeO_2@PDA Nanofiber Textiles with Piezoelectric and Piezo-Phototronic Properties for Self-Powered Piezoelectric Sensor and Photodetector. *Chem. Eng. J.* **2024**, *482*, 148950. [CrossRef]
15. Mineo, G.; Moulaee, K.; Neri, G.; Mirabella, S.; Bruno, E. H_2 Detection Mechanism in Chemoresistive Sensor Based on Low-Cost Synthesized WO_3 Nanorods. *Sens. Actuators B Chem.* **2021**, *348*, 130704. [CrossRef]
16. Rebholz, J.; Weimar, U.; Barsan, N. Influence of Conduction Mechanism Changes on the Sensor Performance of SMOX Based Gas Sensors. *Procedia Eng.* **2014**, *87*, 20–23. [CrossRef]
17. Li, X.; Zhao, Y.; Wang, X.; Wang, J.; Gaskov, A.M.; Akbar, S.A. Reduced Graphene Oxide (rGO) Decorated TiO_2 Microspheres for Selective Room-Temperature Gas Sensors. *Sens. Actuators B Chem.* **2016**, *230*, 330–336. [CrossRef]
18. Lv, D.; Shen, W.; Chen, W.; Wang, Y.; Tan, R.; Zhao, M.; Song, W. Emerging Poly(Aniline Co-Pyrrole) Nanocomposites by in-Situ Polymerized for High-Performance Flexible Ammonia Sensor. *Sens. Actuators A Phys.* **2023**, *349*, 114078. [CrossRef]
19. Yao, P.-C.; Niu, J.-S.; Dai, G.-Y.; Jian, J.-J.; Hsu, W.-C.; Lin, K.-W.; Liu, W.-C. Ammonia Sensing Characteristics of an ITO-V_2O_5 Based Chemoresistive Dual-Type Gas Sensors (CDGS) Decorated with Platinum Nanoparticles. *Sens. Actuators B Chem.* **2023**, *392*, 134071. [CrossRef]
20. Zang, D.; Wei, X.; Liu, Q.; Li, Y.; You, R. In-Situ Growth of ZnO@$ZnWO_4$ Heterojunction with Flower-like Structure by Chemical Vapor Deposition for H_2S Gas Sensor. *Appl. Surf. Sci.* **2025**, *679*, 161149. [CrossRef]

21. Abdulsattar, M.A.; Jabbar, R.H.; Al-Seady, M.A. Ethanol Properties Effects on Its Reaction with Mo-Doped SnO_2 Clusters: A Gas Sensor Model. *Results Surf. Interfaces* **2024**, *17*, 100291. [CrossRef]
22. Chang, Y.-S.; Cheng, M.-C.; Tsai, D.-C.; Shieu, F.-S. Silver nanowires@TiO_2 Core-Shell for Room-Temperature 1000 ppm NH_3 Gas Sensors. *J. Mater. Res. Technol.* **2024**, *31*, 3079–3089. [CrossRef]
23. Kareem, M.H.; Hussein, H.T.; Abdul Hussein, A.M. Study of the Effect of CNTs, and (CNTs-ZnO) on the Porous Silicon as Sensor for Acetone Gas Detection. *Optik* **2022**, *259*, 168825. [CrossRef]
24. Esmaeili, C.; Ashtiani, S.; Regmi, C.; Laposa, A.; Voves, J.; Kroutil, J.; Friess, K.; Povolny, V.; Lotfian, S. Preparation and Characterisation of NH_3 Gas Sensor Based on PANI/Fe-Doped CeO Nanocomposite. *Heliyon* **2024**, *10*, e34801. [CrossRef] [PubMed]
25. Bao, S.; Wu, H.; Chu, X.; Liang, S.; He, L. The Room Temperature Ethanol Gas Sensors Based on MoS_2-$CuGaO_2$ Composite Prepared by Hydrothermal Method. *Talanta* **2024**, *277*, 126287. [CrossRef]
26. Oosthuizen, D.N.; Motaung, D.E.; Swart, H.C. Gas Sensors Based on CeO_2 Nanoparticles Prepared by Chemical Precipitation Method and Their Temperature-Dependent Selectivity towards H_2S and NO_2 Gases. *Appl. Surf. Sci.* **2020**, *505*, 144356. [CrossRef]
27. Khamfoo, K.; Staerz, A.; Boepple, M.; Wisitsoraat, A.; Liewhiran, C.; Weimar, U.; Barsan, N. Operando DRIFT Measurements on Flame-Spray-Made Zn_2SnO_4 Nanoparticles Based Environmental Sensors. *Sens. Actuators B Chem.* **2022**, *371*, 132495. [CrossRef]
28. Yousefi, H.R.; Hashemi, B.; Mirzaei, A.; Roshan, H.; Sheikhi, M.H. Effect of Ag on the ZnO Nanoparticles Properties as an Ethanol Vapor Sensor. *Mater. Sci. Semicond. Process.* **2020**, *117*, 105172. [CrossRef]
29. Chen, C.; Xie, G.; Dai, J.; Li, W.; Cai, Y.; Li, J.; Zhang, Q.; Tai, H.; Jiang, Y.; Su, Y. Integrated Core-Shell Structured Smart Textiles for Active NO_2 Concentration and Pressure Monitoring. *Nano Energy* **2023**, *116*, 108788. [CrossRef]
30. Li, F.; Zhang, T.; Gao, X.; Wang, R.; Li, B. Coaxial Electrospinning Heterojunction SnO_2/Au-Doped In_2O_3 Core-Shell Nanofibers for Acetone Gas Sensor. *Sens. Actuators B Chem.* **2017**, *252*, 822–830. [CrossRef]
31. Walden, R.; Aazem, I.; Hinder, S.; Brennan, B.; Goswami, A.; McGranaghan, G.; Pillai, S.C. Parametric Optimisation of PDMS/PMMA Nanofibers Prepared Using Emulsion Electrospinning Technique. *Results Mater.* **2024**, *22*, 100576. [CrossRef]
32. Switz, A.; Mishra, A.; Jabech, K.; Prasad, A. Affordable Lab-Scale Electrospinning Setup with Interchangeable Collectors for Targeted Fiber Formation. *HardwareX* **2024**, *17*, e00501. [CrossRef] [PubMed]
33. Sukowati, R.; Agung, B.H.; Rohman, Y.M.; Sabandar, M.G.; Waresindo, W.X.; Hapidin, D.A.; Edikresnha, D.; Khairurrijal, K. Optimization of Electrospinning Process Parameters Using Box-Behnken Design for Nylon-6 Nanofibers Fabrication. *Mater. Today Proc.* **2024**, S2214785324001329. [CrossRef]
34. Alagh, A.; Annanouch, F.E.; Umek, P.; Bittencourt, C.; Sierra-Castillo, A.; Haye, E.; Colomer, J.F.; Llobet, E. CVD Growth of Self-Assembled 2D and 1D WS_2 Nanomaterials for the Ultrasensitive Detection of NO_2. *Sens. Actuators B Chem.* **2021**, *326*, 128813. [CrossRef]
35. Yang, J.; Han, W.; Ma, J.; Wang, C.; Shimanoe, K.; Zhang, S.; Sun, Y.; Cheng, P.; Wang, Y.; Zhang, H.; et al. Sn Doping Effect on NiO Hollow Nanofibers Based Gas Sensors about the Humidity Dependence for Triethylamine Detection. *Sens. Actuators B Chem.* **2021**, *340*, 129971. [CrossRef]
36. Walker, J.; Karnati, P.; Akbar, S.A.; Morris, P.A. Selectivity Mechanisms in Resistive-Type Metal Oxide Heterostructural Gas Sensors. *Sens. Actuators B Chem.* **2022**, *355*, 131242. [CrossRef]
37. Bai, H.; Guo, H.; Feng, C.; Wang, J.; Liu, B.; Xie, Z.; Guo, F.; Chen, D.; Zhang, R.; Zheng, Y. A Room-Temperature Chemiresistive NO_2 Sensor Based on One-Step Synthesized SnO_2 Nanospheres Functionalized with Pd Nanoparticles and rGO Nanosheets. *Appl. Surf. Sci.* **2022**, *575*, 151698. [CrossRef]
38. Nam, B.; Ko, T.-K.; Hyun, S.-K.; Lee, C. CO Sensing Properties of Chemiresistive In_2O_3/SnO_2 Composite Nanoparticle Sensors. *J. Nanosci. Nanotechnol.* **2020**, *20*, 4344–4348. [CrossRef]
39. Munsif, S.; Ayub, K.; Nur-e-Alam, M.; Ahmed, S.; Ahmad, A.; Ul-Haq, Z. Sensing of H_2S, NO_2, SO_2, and O_3 through Pristine and Ni-Doped $Zn_{12}O_{12}$ Nanocage. *Comput. Theor. Chem.* **2023**, *1229*, 114305. [CrossRef]
40. Al-Hashem, M.; Akbar, S.; Morris, P. Role of Oxygen Vacancies in Nanostructured Metal-Oxide Gas Sensors: A Review. *Sens. Actuators B Chem.* **2019**, *301*, 126845. [CrossRef]
41. Isaac, N.A.; Pikaar, I.; Biskos, G. Metal Oxide Semiconducting Nanomaterials for Air Quality Gas Sensors: Operating Principles, Performance, and Synthesis Techniques. *Microchim Acta* **2022**, *189*, 196. [CrossRef] [PubMed]
42. Jeong, S.; Kim, J.; Lee, J. Rational Design of Semiconductor-Based Chemiresistors and Their Libraries for Next-Generation Artificial Olfaction. *Adv. Mater.* **2020**, *32*, 2002075. [CrossRef] [PubMed]
43. Ciftyurek, E.; Li, Z.; Schierbaum, K. Adsorbed Oxygen Ions and Oxygen Vacancies: Their Concentration and Distribution in Metal Oxide Chemical Sensors and Influencing Role in Sensitivity and Sensing Mechanisms. *Sensors* **2022**, *23*, 29. [CrossRef]
44. Staerz, A.; Weimar, U.; Barsan, N. Current State of Knowledge on the Metal Oxide Based Gas Sensing Mechanism. *Sens. Actuators B Chem.* **2022**, *358*, 131531. [CrossRef]
45. Hassan, M.; Liang, Z.; Liu, S.; Hussain, S.; Qiao, G.; Liu, G. Temperature-Driven n- to p- type Transition of a Chemiresistive NiO/CdS-CdO NO_2 Gas Sensor. *Sens. Actuators B Chem.* **2024**, *398*, 134755. [CrossRef]
46. Choi, J.H.; Seo, J.S.; Jeong, H.E.; Song, K.; Baeck, S.-H.; Shim, S.E.; Qian, Y. Effects of Field-Effect and Schottky Heterostructure on p-Type Graphene-Based Gas Sensor Modified by n-Type In_2O_3 and Phenylenediamine. *Appl. Surf. Sci.* **2022**, *578*, 152025. [CrossRef]

47. Sinha, M.; Neogi, S.; Mahapatra, R.; Krishnamurthy, S.; Ghosh, R. Material Dependent and Temperature Driven Adsorption Switching (p- to n- type) Using CNT/ZnO Composite-Based Chemiresistive Methanol Gas Sensor. *Sens. Actuators B Chem.* **2021**, *336*, 129729. [CrossRef]
48. Hsu, C.-L.; Chen, K.-C.; Tsai, T.-Y.; Hsueh, T.-J. Fabrication of Gas Sensor Based on p-Type ZnO Nanoparticles and n-Type ZnO Nanowires. *Sens. Actuators B Chem.* **2013**, *182*, 190–196. [CrossRef]
49. Marikutsa, A.; Rumyantseva, M.; Konstantinova, E.A.; Gaskov, A. The Key Role of Active Sites in the Development of Selective Metal Oxide Sensor Materials. *Sensors* **2021**, *21*, 2554. [CrossRef]
50. Giraud, F.; Geantet, C.; Guilhaume, N.; Loridant, S.; Gros, S.; Porcheron, L.; Kanniche, M.; Bianchi, D. Individual Amounts of Lewis and Brønsted Acid Sites on Metal Oxides from NH_3 Adsorption Equilibrium: Case of TiO_2 Based Solids. *Catal. Today* **2021**, *373*, 69–79. [CrossRef]
51. Wu, H.; Huang, H.; Zhou, J.; Hong, D.; Ikram, M.; Rehman, A.U.; Li, L.; Shi, K. One-Step Synthesis of Ordered Pd@TiO_2 Nanofibers Array Film as Outstanding NH_3 Gas Sensor at Room Temperature. *Sci. Rep.* **2017**, *7*, 14688. [CrossRef] [PubMed]
52. Serban, B.-C.; Brezeanu, M.; Cobianu, C.; Costea, S.; Buiu, O.; Stratulat, A.; Varachiu, N. Materials Selection for Gas Sensing. An HSAB Perspective. In Proceedings of the 2014 International Semiconductor Conference (CAS), Sinaia, Romania, 13–15 October 2014; pp. 21–30. [CrossRef]
53. Gole, J.L.; Ozdemir, S. Nanostructure-Directed Physisorption vs. Chemisorption at Semiconductor Interfaces: The Inverse of the HSAB Concept. *ChemPhysChem* **2010**, *11*, 2573–2581. [CrossRef]
54. Gole, J.L.; Ozdemir, S. Novel Concept for the Formation of Sensitive, Selective, Rapidly Responding Conductometric Sensors. *MRS Proc.* **2010**, *1253*, 1253-K07-05. [CrossRef]
55. Wisitsoraat, A.; Tuantranont, A.; Comini, E.; Sberveglieri, G.; Wlodarski, W. Characterization of n-type and p-type Semiconductor Gas Sensors Based on NiO_x Doped TiO_2 Thin Films. *Thin Solid Film.* **2009**, *517*, 2775–2780. [CrossRef]
56. Galatsis, K.; Cukrov, L.; Wlodarski, W.; McCormick, P.; Kalantar-zadeh, K.; Comini, E.; Sberveglieri, G. p- and n-type Fe-Doped SnO_2 Gas Sensors Fabricated by the Mechanochemical Processing Technique. *Sens. Actuators B Chem.* **2003**, *93*, 562–565. [CrossRef]
57. Wang, Y.; Xiao, D.; Zhang, D.; Liu, Y.; Sun, M.; Sun, M.; Li, J. Construction of Ag_2O/WO_3-Based Hollow Microsphere p-n Heterojunction for Continuous Detection of ppb-Level H_2S Gas Sensor. *J. Alloys Compd.* **2024**, *1003*, 175735. [CrossRef]
58. Ding, Y.; Du, B.; Guo, X.; Dong, Y.; Zhang, M.; Jin, W.; Gao, C.; Peng, D.; He, Y. An Ultrasensitive NO_2 Gas Sensor Based on a NiO-SnO_2 Composite with a Sub-ppb Detection Limit at Room Temperature. *Sens. Actuators B Chem.* **2024**, *414*, 135916. [CrossRef]
59. Cai, Z.; Park, S. Fabrication of Selective and Highly Sensitive Triethylamine Gas Sensor Using In_2O_3–SnO_2 Hollow Nanospheres in Room Temperature Activated by UV Irradiation. *J. Mater. Res. Technol.* **2023**, *26*, 6581–6596. [CrossRef]
60. Lee, J.; Gam, D.-Y.; Nam, K.E.; Cho, S.J.; Kim, H. Feasibility Study of a Resistive-Type Sodium Aerosol Detector with ZnO Nanowires for Sodium-Cooled Fast Reactors. *Nucl. Eng. Technol.* **2023**, *55*, 2373–2379. [CrossRef]
61. Hongsith, N.; Chansuriya, S.; Koenrobket, S.; Unai, S.; Wongrat, E.; Prasatkhetragarn, A. Investigating of Transition State on the Pd–Au Decorated ZnO Nanoparticle Layers for Gas Sensor Application. *Heliyon* **2023**, *9*, e19402. [CrossRef]
62. Li, S.; He, J.; Man, Y.; Li, L.; Li, S.; Li, N.; Zhao, Q. A First-Principles Study into Pt-Embedded NiS_2 Monolayer as an Outstanding Gas Sensor upon CO and HCHO Dry-Type Reactors. *Comput. Theor. Chem.* **2023**, *1226*, 114203. [CrossRef]
63. Tian, X.; Yin, M.; Zhang, L.; Qiu, T.; Xu, D.; Qiu, J. Mesoporous ZnO@CO_3O_4 Nanosphere for Sensitive Detection of 3-Hydroxy-2-Butanone. *J. Photochem. Photobiol.* **2022**, *11*, 100135. [CrossRef]
64. To, D.T.H.; Park, J.Y.; Yang, B.; Myung, N.V.; Choa, Y.-H. Nanocrystalline ZnO Quantum Dot-Based Chemiresistive Gas Sensors: Improving Sensing Performance towards NO_2 and H_2S by Optimizing Operating Temperature. *Sens. Actuators Rep.* **2023**, *6*, 100166. [CrossRef]
65. Fadojutimi, P.; Masemola, C.; Nkabinde, S.S.; Maubane-Nkadimeng, M.; Linganiso, E.C.; Tetana, Z.N.; Moloto, N.; Moma, J.; Gqoba, S. Room Temperature Sensing of Alcohol Vapours Using Novel Radially Aligned Nanorutile Titania. *Sens. Actuators Rep.* **2023**, *5*, 100154. [CrossRef]
66. Alfalasi, W.; Feng, Y.P.; Tit, N. Designing a Functionalized 2D-TMD (MoX_2, X = S, Se) Hosting Half-Metallicity for Selective Gas-Sensing Applications: Atomic-Scale Study. *Acta Mater.* **2023**, *246*, 118655. [CrossRef]
67. Luo, S.; Chen, R.; Wang, J.; Xiang, L. Conductometric Methane Gas Sensors Based on ZnO/Pd@ZIF-8: Effect of Dual Filtering of ZIF-8 to Increase the Selectivity. *Sens. Actuators B Chem.* **2023**, *383*, 133600. [CrossRef]
68. Lee, J.; Kim, H.; Hilal, M.; Cai, Z. Core–Shell SnO_2/NiO p–n Heterojunction Composite for Enhanced Triethylamine Gas Sensitivity and Selectivity. *J. Mater. Sci. Mater. Electron.* **2024**, *35*, 1421. [CrossRef]
69. Kumar, M.; Sharma, S.; Pal, R.; Vidhani, B.; Supreet. A Novel Gas Sensor Based on Activated Charcoal and Polyaniline Composites for Selective Sensing of Methanol Vapors. *Sens. Actuators A Phys.* **2023**, *353*, 114210. [CrossRef]
70. Kumar, S.; Lawaniya, S.D.; Agarwal, S.; Yu, Y.-T.; Nelamarri, S.R.; Kumar, M.; Mishra, Y.K.; Awasthi, K. Optimization of Pt Nanoparticles Loading in ZnO for Highly Selective and Stable Hydrogen Gas Sensor at Reduced Working Temperature. *Sens. Actuators B Chem.* **2023**, *375*, 132943. [CrossRef]
71. Singh, S.; Adalati, R.; Gurawal, P.; Malik, G.; Kaur, D.; Chandra, R. Highly Efficient NO_2 Gas Sensor Based on Sputter-Grown Nanocrystalline MoO_3 Thin Films. *Mater. Lett.* **2024**, *369*, 136762. [CrossRef]
72. Kim, K.B.; Moon, Y.K.; Kim, T.-H.; Yu, B.-H.; Li, H.-Y.; Kang, Y.C.; Yoon, J.-W. Highly Selective and Sensitive Detection of Carcinogenic Benzene Using a Raisin Bread-Structured Film Comprising Catalytic Pd-Co_3O_4 and Gas-Sensing SnO_2 Hollow Spheres. *Sens. Actuators B Chem.* **2023**, *386*, 133750. [CrossRef]

73. Hong, J.; Lee, S.; Seo, J.; Pyo, S.; Kim, J.; Lee, T. A Highly Sensitive Hydrogen Sensor with Gas Selectivity Using a PMMA Membrane-Coated Pd Nanoparticle/Single-Layer Graphene Hybrid. *ACS Appl. Mater. Interfaces* **2015**, *7*, 3554–3561. [CrossRef] [PubMed]
74. Domènech-Gil, G.; Samà, J.; Fàbrega, C.; Gràcia, I.; Cané, C.; Barth, S.; Romano-Rodríguez, A. Highly Sensitive SnO_2 Nanowire Network Gas Sensors. *Sens. Actuators B Chem.* **2023**, *383*, 133545. [CrossRef]
75. Singh, M.; Kaur, N.; Casotto, A.; Sangaletti, L.; Comini, E. Tailoring the Surface Chemistry of ZnO Nanowires via Mixed Self-Assembly of Organosilanes for Selective Acetone Detection. *Sens. Actuators B Chem.* **2023**, *384*, 133653. [CrossRef]
76. Kwon, Y.M.; Oh, B.; Purbia, R.; Chae, H.Y.; Han, G.H.; Kim, S.-W.; Choi, K.-J.; Lee, Y.; Kim, J.J.; Baik, J.M. High-Performance and Self-Calibrating Multi-Gas Sensor Interface to Trace Multiple Gas Species with Sub-Ppm Level. *Sens. Actuators B Chem.* **2023**, *375*, 132939. [CrossRef]
77. Plugotarenko, N.K.; Myasoedova, T.N.; Novikov, S.P.; Mikhailova, T.S. Comparative Analysis of Derivative Parameters of Chemoresistive Sensor Signals for Gas Concentration Estimation. *Chemosensors* **2022**, *10*, 126. [CrossRef]
78. Suriyawong, S.; Khumphon, J.; Rattanakam, R.; Chaopanich, P.; Thongmee, S.; Youngjan, S.; Khemthong, P.; Kityakarn, S. Engineering Three-Dimensionally Ordered Mesoporous Structure of TiO_2 for the Fast Responsive NH_3 Gas Sensor at Ambient Conditions. *Colloids Surf. A Physicochem. Eng. Asp.* **2023**, *666*, 131281. [CrossRef]
79. Qiu, P.; Qin, Y.; Zhu, L. Memristive Gas Sensor (Gasistor) Based on Ag/Ordered TiO_2 Nanorods/FTO Sandwich Structure for Evaluation of Ethanol Concentration in Mixed Ambient. *Sens. Actuators B Chem.* **2024**, *421*, 136548. [CrossRef]
80. Meng, F.; Li, G.; Ji, H.; Shen, Y.; Yuan, Z. Detection and Identification of the Gas Mixtures of N-Propyl Alcohol and Iso-Propyl Alcohol Based on ZnO Sensor under Dynamic Temperature Modulation. *Sens. Actuators B Chem.* **2025**, *422*, 136583. [CrossRef]
81. Goel, N.; Kunal, K.; Kushwaha, A.; Kumar, M. Metal Oxide Semiconductors for Gas Sensing. *Eng. Rep.* **2023**, *5*, e12604. [CrossRef]
82. Huo, X.; Shan, X.; Pan, Q.; Cao, Z.; Cong, Z.; Song, J.; Jiang, J.; Ma, Q.; Jia, L.; Gao, J. Solution-Processable Quinoidal Compounds Containing Heterocycle for Air-Stable N-type Organic Field-Effect Transistors and Gas Sensors. *Sens. Actuators B Chem.* **2024**, *403*, 135184. [CrossRef]
83. Vishnuraj, R.; Karuppanan, K.K.; Aleem, M.; Pullithadathil, B. Boosting the Performance of NO_2 Gas Sensors Based on n–n Type Mesoporous ZnO@In_2O_3 Heterojunction Nanowires: In Situ Conducting Probe Atomic Force Microscopic Elucidation of Room Temperature Local Electron Transport. *Nanoscale Adv.* **2020**, *2*, 4785–4797. [CrossRef] [PubMed]
84. Mao, J.N.; Hong, B.; Chen, H.D.; Gao, M.H.; Xu, J.C.; Han, Y.B.; Yang, Y.T.; Jin, H.X.; Jin, D.F.; Peng, X.L.; et al. Highly Improved Ethanol Gas Response of N-Type α-Fe_2O_3 Bunched Nanowires Sensor with High-Valence Donor-Doping. *J. Alloys Compd.* **2020**, *827*, 154248. [CrossRef]
85. Chiu, C.-C.; Kuo, C.-K.; Chu, P.-Y.; Shih, D.-H.; Liu, W.-C. Study of a Palladium Nanoparticle/ In-Zn-O Thin Film-Based Hydrogen Gas Sensor. *Sens. Actuators B Chem.* **2024**, *415*, 136015. [CrossRef]
86. Wu, X.; Xiong, S.; Gong, Y.; Gong, Y.; Wu, W.; Mao, Z.; Liu, Q.; Hu, S.; Long, X. MOF-SMO Hybrids as a H_2S Sensor with Superior Sensitivity and Selectivity. *Sens. Actuators B Chem.* **2019**, *292*, 32–39. [CrossRef]
87. Park, H.; Kim, J.-H.; Vivod, D.; Kim, S.; Mirzaei, A.; Zahn, D.; Park, C.; Kim, S.S.; Halik, M. Chemical-Recognition-Driven Selectivity of SnO_2-Nanowire-Based Gas Sensors. *Nano Today* **2021**, *40*, 101265. [CrossRef]
88. Yang, L.; Qin, J.; Cui, S.; Liu, W. Silver Nanoparticle Functionalized Heterojunction NiO/SnO_2 Nanotubes for Comprehensive Sensitization of Acetone Sensor. *Sens. Actuators B Chem.* **2024**, *417*, 136208. [CrossRef]
89. Adhikari, A.; Tiwary, P.; Rana, D.; Halder, A.; Nath, J.; Basu, A.; Ghoshal, D.; Kar, P.; Chakraborty, A.K.; Chattopadhyay, D. Na-Cholate Micelle Mediated Synthesis of Polypyrrole Nanoribbons for Ethanol Sensing. *J. Environ. Chem. Eng.* **2020**, *8*, 104249. [CrossRef]
90. Travlou, N.A.; Rodríguez-Castellón, E.; Bandosz, T.J. Sensing of NH_3 on Heterogeneous Nanoporous Carbons in the Presence of Humidity. *Carbon* **2016**, *100*, 64–73. [CrossRef]
91. Golovakhin, V.; Litvinova, V.I.; Manakhov, A.; Latypova, A.R.; Novgorodtseva, O.N.; Ukhina, A.V.; Ishchenko, A.V.; Al-Qasim, A.S.; Maksimovskiy, E.A.; Bannov, A.G. Conductive Polymer-Multi-Walled Carbon Nanotube Composites for Gas Sensors and Supercapacitors. *Mater. Today Commun.* **2024**, *39*, 109163. [CrossRef]
92. Zhang, J.; Maimaitiyiming, X. Study on Phenyl Series of Polymers Wrapping of Different Diameters of Semiconducting Single-Walled Carbon Nanotubes for Ammonia Gas Sensors. *Sens. Actuators B Chem.* **2024**, *405*, 135278. [CrossRef]
93. Wang, S.; Cao, J.; Zhao, Y.; Liu, X.; Guo, Y.; Chen, J.; Wang, W.; Zhang, R.; Zhang, Y.; Liu, X.; et al. Influence of Pt or Au Doping on Improving the Detection of CO by ZnO: A First-Principles Calculations Study. *Chem. Phys.* **2023**, *570*, 111908. [CrossRef]
94. Szary, M.J. Toward High Selectivity of Sensor Arrays: Enhanced Adsorption Interaction and Selectivity of Gas Detection (N_2, O_2, NO, CO, CO_2, NO_2, SO_2, AlH_3, NH_3, and PH_3) on Transition Metal Dichalcogenides (MoS_2, $MoSe_2$, and $MoTe_2$). *Acta Mater.* **2024**, *274*, 120016. [CrossRef]
95. Parangusan, H.; Bhadra, J.; Al-Qudah, R.A.; Elhadrami, E.C.; Al-Thani, N.J. Comparative Study on Gas-Sensing Properties of 2D (MoS_2, WS_2)/PANI Nanocomposites-Based Sensor. *Nanomaterials* **2022**, *12*, 4423. [CrossRef]
96. Kumar, A.N.; Pal, K. Amine-Functionalized Stable Nb_2CT_x MXene toward Room Temperature Ultrasensitive NO_2 Gas Sensor. *Mater. Adv.* **2022**, *3*, 5151–5162. [CrossRef]
97. Song, X.; Liu, T.; Gu, K.; Luo, Z.; Zhang, M. Highly Selective and Ultra-Sensitive Gas Sensor Based on Fe_2O_3/$Ti_3C_2T_x$ MXene Heterostructure for ppb-level n-butanol Detection. *J. Alloys Compd.* **2024**, *976*, 173153. [CrossRef]

98. Casanova-Chafer, J.; Garcia-Aboal, R.; Atienzar, P.; Llobet, E. Unraveling the Gas-Sensing Mechanisms of Lead-Free Perovskites Supported on Graphene. *ACS Sens.* **2022**, *7*, 3753–3763. [CrossRef]
99. Xie, T.; Li, F.; Song, P.; Fang, M.; Duan, L.; Zhang, Q.; Geng, W. High Responsive n-butanol Gas Sensor Based on MOFs-Derived Cr_2O_3/RGO p-p Heterojunctions Materials. *J. Alloys Compd.* **2024**, *1002*, 175271. [CrossRef]
100. Montoro, C.; Kim, J.-Y.; Mirzaei, A.; Lee, J.-H.; Sayegh, S.; Makhoul, E.; Iatsunskyi, I.; Coy, E.; Bechelany, M.; Kim, H.W.; et al. MOF-Derived Metal Oxide (Cu, Ni, Zn) Gas Sensors with Excellent Selectivity towards H_2S, CO and H_2 Gases. *Compos. Part B Eng.* **2024**, *283*, 111637. [CrossRef]
101. Shah, S.; Hussain, S.; Khan, L.A.; Yusuf, K.; Manavalan, R.K.; Tianyan, Y.; Zhang, X.; Liu, G.; Qiao, G. ppb-Level H_2 Gas-Sensor Based on Porous Ni-MOF Derived NiO@CuO Nanoflowers for Superior Sensing Performance. *Mater. Res. Bull.* **2024**, *180*, 113021. [CrossRef]
102. Matatagui, D.; Sainz-Vidal, A.; Gràcia, I.; Figueras, E.; Cané, C.; Saniger, J.M. Chemoresistive Gas Sensor Based on ZIF-8/ZIF-67 Nanocrystals. *Sens. Actuators B Chem.* **2018**, *274*, 601–608. [CrossRef]
103. Kandhare, N.; Mathe, V.L.; Bhagwat, S. Room Temperature NO_2 Gas Sensor Using H-WO_3 Nanorod Based Thin Films. *Mater. Sci. Eng. B* **2024**, *305*, 117422. [CrossRef]
104. Lv, H.; Dai, J.; Fang, O.; Wang, A.; Sun, W.; Liu, Z. Structure-Dependent Biomorphology Co_3O_4-In_2O_3 Nanorods for Expired Acetone Gas Sensor. *Surf. Interfaces* **2024**, *49*, 104376. [CrossRef]
105. Lai, L.-T.; Hsueh, H.-T.; Chiu, C.-H.; Cheng, T.-C.; Chang, S.-J. Thermal Oxidation CuO Nanowire Gas Sensor for Ozone Detection Applications. *Sens. Actuators Rep.* **2024**, *8*, 100228. [CrossRef]
106. Yang, X.; Zhang, S.; Yu, Q.; Zhao, L.; Sun, P.; Wang, T.; Liu, F.; Yan, X.; Gao, Y.; Liang, X.; et al. One Step Synthesis of Branched SnO_2/ZnO Heterostructures and Their Enhanced Gas-Sensing Properties. *Sens. Actuators B Chem.* **2019**, *281*, 415–423. [CrossRef]
107. Ghorbani, G.; Taghipour, F. UV-Activated Chemiresistive Gas Sensor Response Curve Analysis for the Fast Measurement of Toxic Gases. *Sens. Actuators B Chem.* **2024**, *419*, 136396. [CrossRef]
108. Cai, Z.; Goo, E.; Park, S. Hydrogen Sensing Performance and Its Enhanced Sensing Mechanisms of Hollow Structured-SnO2 Nanospheres Activated by Noble Metal Nanoparticles. *J. Mater. Res. Technol.* **2021**, *15*, 1716–1731. [CrossRef]
109. Ramanathan, R.; Nagarajan, S.; Sathiyamoorthy, S.; Manavaimaran, B.; Barshilia, H.C.; Mallik, R.C. A Highly Sensitive and Room Temperature Ethanol Gas Sensor Based on Spray Deposited Sb Doped SnO_2 Thin Films. *Mater. Adv.* **2024**, *5*, 293–305. [CrossRef]
110. Kou, X.; Xie, N.; Chen, F.; Wang, T.; Guo, L.; Wang, C.; Wang, Q.; Ma, J.; Sun, Y.; Zhang, H.; et al. Superior Acetone Gas Sensor Based on Electrospun SnO_2 Nanofibers by Rh Doping. *Sens. Actuators B Chem.* **2018**, *256*, 861–869. [CrossRef]
111. Van Hoang, N.; Hung, C.M.; Hoa, N.D.; Van Duy, N.; Van Hieu, N. Facile On-Chip Electrospinning of $ZnFe_2O_4$ Nanofiber Sensors with Excellent Sensing Performance to H_2S down ppb Level. *J. Hazard. Mater.* **2018**, *360*, 6–16. [CrossRef]
112. Han, L.; Zhang, S.; Zhang, B.; Zhang, B.; Wang, Y.; Bala, H.; Zhang, Z. Dual-Selective Detection of CO and CH_4 Based on Hierarchical Porous In_2O_3 Nanoflowers with Pd Modification. *J. Mater.* **2022**, *8*, 545–555. [CrossRef]
113. Krishnakumar, T.; Jayaprakash, R.; Pinna, N.; Donato, N.; Bonavita, A.; Micali, G.; Neri, G. CO Gas Sensing of ZnO Nanostructures Synthesized by an Assisted Microwave Wet Chemical Route. *Sens. Actuators B Chem.* **2009**, *143*, 198–204. [CrossRef]
114. Wei, S.; Yu, Y.; Zhou, M. CO Gas Sensing of Pd-Doped ZnO Nanofibers Synthesized by Electrospinning Method. *Mater. Lett.* **2010**, *64*, 2284–2286. [CrossRef]
115. Altinkok, C.; Sagdic, G.; Daglar, O.; Ercan Ayra, M.; Yuksel Durmaz, Y.; Durmaz, H.; Acik, G. A New Strategy for Direct Solution Electrospinning of Phosphorylated Poly(Vinyl Chloride)/Polyethyleneimine Blend in Alcohol Media. *Eur. Polym. J.* **2023**, *183*, 111750. [CrossRef]
116. Perez-Puyana, V.M.; Romero, A.; Guerrero, A.; Moroni, L.; Wieringa, P.A. Enabling Low Molecular Weight Electrospinning through Binary Solutions of Polymer Blends. *Next Mater.* **2025**, *6*, 100306. [CrossRef]
117. Joy, N.; Anuraj, R.; Viravalli, A.; Dixit, H.N.; Samavedi, S. Coupling between Voltage and Tip-to-Collector Distance in Polymer Electrospinning: Insights from Analysis of Regimes, Transitions and Cone/Jet Features. *Chem. Eng. Sci.* **2021**, *230*, 116200. [CrossRef]
118. Singh, R.K.; Lye, S.W.; Miao, J. Holistic Investigation of the Electrospinning Parameters for High Percentage of β-Phase in PVDF Nanofibers. *Polymer* **2021**, *214*, 123366. [CrossRef]
119. Rosman, N.; Wan Salleh, W.N.; Jamalludin, M.R.; Adam, M.R.; Ismail, N.H.; Jaafar, J.; Harun, Z.; Ismail, A.F. Electrospinning Parameters Evaluation of PVDF-ZnO/Ag_2CO_3/Ag_2O Composite Nanofiber Affect on Porosity by Using Response Surface Methodology. *Mater. Today Proc.* **2021**, *46*, 1824–1830. [CrossRef]
120. Chen, L.; Yu, Q.; Pan, C.; Song, Y.; Dong, H.; Xie, X.; Li, Y.; Liu, J.; Wang, D.; Chen, X. Chemiresistive Gas Sensors Based on Electrospun Semiconductor Metal Oxides: A Review. *Talanta* **2022**, *246*, 123527. [CrossRef]
121. Xiong, J.; Liu, Y.; Li, A.; Wei, L.; Wang, L.; Qin, X.; Yu, J. Mass Production of High-Quality Nanofibers via Constructing Pre-Taylor Cones with High Curvature on Needleless Electrospinning. *Mater. Des.* **2021**, *197*, 109247. [CrossRef]
122. Martin, P.; Zussman, E. Charge Transport in Electrospinning of Polyelectrolyte Solutions. *Soft Matter* **2024**, *20*, 5572–5582. [CrossRef] [PubMed]
123. Singh, S.K.; Sarma, S. Taylor Cone Height as a Tool to Understand Properties of Electrospun PVDF Nanofibers. *J. Electrost.* **2022**, *120*, 103770. [CrossRef]
124. Di Bonito, L.P.; Kyriacou, P.; Di Colandrea, A.; Di Natale, F.; Ruoppolo, G.; Krasia-Christoforou, T. Design and Production of Functionalized Electrospun Fibers for Palladium Recovery. *ACS Appl. Polym. Mater.* **2024**, *6*, 9406–9419. [CrossRef] [PubMed]

125. Beachley, V.; Wen, X. Effect of Electrospinning Parameters on the Nanofiber Diameter and Length. *Mater. Sci. Eng. C* **2009**, *29*, 663–668. [CrossRef]
126. Kočí, J.; Míka Havlík, M.; Procházka, V.; Klusoňová, N.; Sedláčková, E. The Effect of Solution Viscosity on the Quality of Electroactive Nanofibers Produced by Electrospinning. *Monatsh. Chem.* **2024**, *155*, 349–352. [CrossRef]
127. Rajeev, M.; Helms, C.C. A Study of the Relationship between Polymer Solution Entanglement and Electrospun PCL Fiber Mechanics. *Polymers* **2023**, *15*, 4555. [CrossRef]
128. Rabello, L.G.; Alvares, M.R.N.; Ribeiro, R.C.D.C.; Jardim, P.M.; Thiré, R.M.D.S.M. Correlation between Solution Relative Viscosity and the Microstructural Properties of the Poly(3-Hydroxybutyrate-Co-3-Hydroxyvalerate)—PHBV Solution Blow Spun Mats. *Express Polym. Lett.* **2023**, *17*, 1239–1256. [CrossRef]
129. Ewaldz, E.; Randrup, J.; Brettmann, B. Solvent Effects on the Elasticity of Electrospinnable Polymer Solutions. *ACS Polym. Au* **2022**, *2*, 108–117. [CrossRef]
130. Liu, Z.; Ramakrishna, S.; Ahmed, I.; Rudd, C.; Liu, X. Rheological, Surface Tension and Conductivity Insights on the Electrospinnability of Poly(Lactic-Co-Glycolic Acid)-Hyaluronic Acid Solutions and Their Correlations with the Nanofiber Morphological Characteristics. *Polymers* **2022**, *14*, 4411. [CrossRef]
131. Rathore, P.; Schiffman, J.D. Effect of pH Value on the Electrical Properties of PEDOT:PSS-Based Fiber Mats. *ACS Eng. Au* **2023**, *3*, 527–536. [CrossRef]
132. Ruiz Rocha, J.E.; Moreno Tovar, K.R.; Navarro Mendoza, R.; Gutiérrez Granados, S.; Cavaliere, S.; Giaume, D.; Barboux, P.; Jaime Ferrer, J.S. Critical Electrospinning Parameters for Synthesis Control of Stabilized Polyacrylonitrile Nanofibers. *Nanomaterials* **2023**, *13*, 2648. [CrossRef] [PubMed]
133. Sheikhi, S.; Ghassemi, A.; Sajadi, S.M.; Hashemian, M. Comparison of the Mechanical Characteristics of Produced Nanofibers by Electrospinning Process Based on Different Collectors. *Heliyon* **2024**, *10*, e23841. [CrossRef] [PubMed]
134. Ura, D.P.; Stachewicz, U. Direct Electrospinning of Short Polymer Fibers: Factors Affecting Size and Quality. *Compos. Part A Appl. Sci. Manuf.* **2024**, *181*, 108138. [CrossRef]
135. SalehHudin, H.S.; Mohamad, E.N.; Afifi, A.M.; Mahadi, W.N.L.W. Simulation and Experimental Study of Parameters in Multiple-Nozzle Electrospinning: Effects of Voltage and Nozzle Configuration on the Electric Field and Electrospun Jet Attributes. *J. Manuf. Process.* **2023**, *85*, 544–555. [CrossRef]
136. Najim, M.A.; Khalil, B.I.; Hameed, A.A. Characterizing Optimum Electrospinning Conditions for Graft Urethanized Poly(Vinyl Alcohol)(U-PVA). *Heliyon* **2022**, *8*, e11423. [CrossRef]
137. Su, Y.; Zhang, Z.; Wang, Z.; Chen, M.; Dong, M.; Han, X. Necklace-like Fiber Composite Membrane for High-Efficiency Particulate Matter Capture. *Appl. Surf. Sci.* **2017**, *425*, 220–226. [CrossRef]
138. Ghosh, S.; Yadav, A.; Gurave, P.M.; Srivastava, R.K. Unique Fiber Morphologies from Emulsion Electrospinning—A Case Study of Poly(ε-Caprolactone) and Its Applications. *Colloids Interfaces* **2023**, *7*, 19. [CrossRef]
139. Zaarour, B.; Zhu, L.; Huang, C.; Jin, X. Controlling the Secondary Surface Morphology of Electrospun PVDF Nanofibers by Regulating the Solvent and Relative Humidity. *Nanoscale Res. Lett.* **2018**, *13*, 285. [CrossRef] [PubMed]
140. Fatimah, I.; Sari, T.I.; Anggoro, D. Effect of Concentration and Nozzle-Collector Distance on the Morphology of Nanofibers. *KEM* **2020**, *860*, 315–319. [CrossRef]
141. Hoogesteijn Von Reitzenstein, N.; Sonmez Baghirzade, B.; Pruitt, E.; Hristovski, K.; Westerhoff, P.; Apul, O.G. Comparing the Morphologies and Adsorption Behavior of Electrospun Polystyrene Composite Fibers with 0D Fullerenes, 1D Multiwalled Carbon Nanotubes and 2D Graphene Oxides. *Chem. Eng. J. Adv.* **2022**, *9*, 100199. [CrossRef]
142. Fioravanti, A.; Morandi, S.; Pedrazzo, A.R.; Cecone, C.; Manzoli, M.; Zanetti, M.; Bracco, P.; Mazzocchi, M.; Lettieri, S.; Marani, P.; et al. Investigation of the Key Parameters for Gas Sensing through Comparison of Electrospun and Sol-Gel Semiconducting Oxides. *Ceram. Int.* **2022**, *48*, 20948–20960. [CrossRef]
143. Phuoc, P.H.; Van Hoang, N.; Hung, N.M.; Hung, P.T.; Hoat, P.D.; Van Hieu, N. On-Chip $CuFe_2O_4$ Nanofiber for Conductometric NO_2 and H_2S Gas-Sensors. *Sens. Actuators B Chem.* **2023**, *380*, 133306. [CrossRef]
144. Reddy, C.S.; Murali, G.; Reddy, A.S.; Park, S.; In, I. GO Incorporated SnO_2 Nanotubes as Fast Response Sensors for Ethanol Vapor in Different Atmospheres. *J. Alloys Compd.* **2020**, *813*, 152251. [CrossRef]
145. Platonov, V.; Rumyantseva, M.; Khmelevsky, N.; Gaskov, A. Electrospun ZnO/Pd Nanofibers: CO Sensing and Humidity Effect. *Sensors* **2020**, *20*, 7333. [CrossRef] [PubMed]
146. Liu, W.; Xie, Y.; Chen, T.; Lu, Q.; Ur Rehman, S.; Zhu, L. Rationally Designed Mesoporous In_2O_3 Nanofibers Functionalized Pt Catalysts for High-Performance Acetone Gas Sensors. *Sens. Actuators B Chem.* **2019**, *298*, 126871. [CrossRef]
147. Hong, S.-Z.; Huang, Q.-Y.; Wu, T.-M. The Room Temperature Highly Sensitive Ammonia Gas Sensor Based on Polyaniline and Nitrogen-Doped Graphene Quantum Dot-Coated Hollow Indium Oxide Nanofiber Composite. *Polymers* **2021**, *13*, 3676. [CrossRef]
148. Sharma, H.J.; Jamkar, D.V.; Kondawar, S.B. Electrospun Nanofibers of Conducting Polyaniline/Al-SnO_2 Composites for Hydrogen Sensing Applications. *Procedia Mater. Sci.* **2015**, *10*, 186–194. [CrossRef]
149. Andre, R.; Kwak, D.; Dong, Q.; Zhong, W.; Correa, D.; Mattoso, L.; Lei, Y. Sensitive and Selective NH_3 Monitoring at Room Temperature Using ZnO Ceramic Nanofibers Decorated with Poly(Styrene Sulfonate). *Sensors* **2018**, *18*, 1058. [CrossRef]
150. Lee, J.-H.; Kim, J.-Y.; Kim, J.-H.; Kim, S. Enhanced Hydrogen Detection in ppb-Level by Electrospun SnO_2-Loaded ZnO Nanofibers. *Sensors* **2019**, *19*, 726. [CrossRef]

151. Platonov, V.; Nasriddinov, A.; Rumyantseva, M. Electrospun ZnO/Pd Nanofibers as Extremely Sensitive Material for Hydrogen Detection in Oxygen Free Gas Phase. *Polymers* **2022**, *14*, 3481. [CrossRef]
152. Cai, Z.; Park, J.; Park, S. Porous In_2O_3–ZnO Nanofiber-Based Sensor for Ultrasensitive Room-Temperature Detection of Toluene Gas under UV Illumination. *J. Mater. Res. Technol.* **2023**, *24*, 2482–2499. [CrossRef]
153. Korotcenkov, G.; Cho, B.K. The Role of Grain Size on the Thermal Instability of Nanostructured Metal Oxides Used in Gas Sensor Applications and Approaches for Grain-Size Stabilization. *Prog. Cryst. Growth Charact. Mater.* **2012**, *58*, 167–208. [CrossRef]
154. Song, L.; Yang, L.; Wang, Z.; Liu, D.; Luo, L.; Zhu, X.; Xi, Y.; Yang, Z.; Han, N.; Wang, F.; et al. One-Step Electrospun SnO_2/MOx Heterostructured Nanomaterials for Highly Selective Gas Sensor Array Integration. *Sens. Actuators B Chem.* **2019**, *283*, 793–801. [CrossRef]
155. Zhu, L.; Wang, Z.; Wang, J.; Liu, J.; Zhao, W.; Zhang, J.; Yan, W. Synergistic Effect of ZIF-8 and Pt-Functionalized NiO/In_2O_3 Hollow Nanofibers for Highly Sensitive Detection of Formaldehyde. *Nanomaterials* **2024**, *14*, 841. [CrossRef] [PubMed]
156. Lu, Z.; Zhou, Q.; Wang, C.; Wei, Z.; Xu, L.; Gui, Y. Electrospun ZnO–SnO_2 Composite Nanofibers and Enhanced Sensing Properties to SF_6 Decomposition Byproduct H_2S. *Front. Chem.* **2018**, *6*, 540. [CrossRef]
157. Liu, W.; Xu, L.; Sheng, K.; Zhou, X.; Dong, B.; Lu, G.; Song, H. A Highly Sensitive and Moisture-Resistant Gas Sensor for Diabetes Diagnosis with Pt@In_2O_3 Nanowires and a Molecular Sieve for Protection. *NPG Asia Mater.* **2018**, *10*, 293–308. [CrossRef]
158. Shao, H.; Huang, M.; Fu, H.; Wang, S.; Wang, L.; Lu, J.; Wang, Y.; Yu, K. Hollow WO_3/SnO_2 Hetero-Nanofibers: Controlled Synthesis and High Efficiency of Acetone Vapor Detection. *Front. Chem.* **2019**, *7*, 785. [CrossRef]
159. Avossa, J.; Paolesse, R.; Di Natale, C.; Zampetti, E.; Bertoni, G.; De Cesare, F.; Scarascia-Mugnozza, G.; Macagnano, A. Electrospinning of Polystyrene/Polyhydroxybutyrate Nanofibers Doped with Porphyrin and Graphene for Chemiresistor Gas Sensors. *Nanomaterials* **2019**, *9*, 280. [CrossRef]
160. Wu, W.-Y.; Ting, J.-M.; Huang, P.-J. Electrospun ZnO Nanowires as Gas Sensors for Ethanol Detection. *Nanoscale Res. Lett.* **2009**, *4*, 513. [CrossRef]
161. Sun, H.; Yao, Y.; Yang, R.; Yan, Z.; Cao, C.; Deng, Y.; Wu, S.; Liu, S.; Xu, Q.; Qin, Y. A ZnO Gas Sensor with an Abnormal Response to Hydrogen. *Energies* **2023**, *16*, 5847. [CrossRef]
162. Du, X.; Xing, R.; Lin, Y.; Chen, M.; Chen, Z.; Zhou, S. Reduced Greenhouse Gas Emission by Reactive Oxygen Species during Composting. *Bioresour. Technol.* **2024**, *404*, 130910. [CrossRef] [PubMed]
163. Kashyap, A.; Bir Barman, P.; Kumar Hazra, S. Role of Catalyst Oxidation States in the Selective Detection of Reducing Gases: A Comparative Study of Nanocomposites Based on Au and Chemically/Thermally Reduced Graphene Oxide. *Mater. Sci. Eng. B* **2024**, *308*, 117605. [CrossRef]
164. Jiang, D.; Chen, Q.; Ding, D.; Zhou, Y.; Xie, W.; Xia, F.; Li, M.; Wei, J.; Chen, Y.; Deng, S. Derivation of Human Health and Odor Risk Control Values for Soil Ammonia Nitrogen by Incorporating Solid-Liquid Partitioning, Ammonium/Ammonia Equilibrium: A Case Study of a Retired Nitrogen Fertilizer Site in China. *Ecotoxicol. Environ. Saf.* **2024**, *273*, 116133. [CrossRef] [PubMed]
165. Zhao, H.; He, X.; Shi, Z.; Li, S. Adsorption and Sensing Behavior of Cr-Doped WS_2 Monolayer for Hazardous Gases in Agricultural Greenhouses: A DFT Study. *Mater. Today Commun.* **2024**, *40*, 109405. [CrossRef]
166. Cheng, Y.-F.; Song, S.-X.; Ma, H.-H.; Su, J.; Han, T.-F.; Shen, Z.-W.; Meng, X.-R. Hybrid H_2/Ti Dust Explosion Hazards during the Production of Metal Hydride TiH_2 in a Closed Vessel. *Int. J. Hydrogen Energy* **2019**, *44*, 11145–11152. [CrossRef]
167. Jimenez, A.; Groth, K.M. Hazards Associated with Pressure Relief Devices in Hydrogen Systems. *J. Loss Prev. Process Ind.* **2024**, *91*, 105380. [CrossRef]
168. Zhang, J.; Li, T.; Zhang, H.; Huang, Z.; Zeng, W.; Zhou, Q. Ni Decorated ReS_2 Monolayer as Gas Sensor or Adsorbent for Agricultural Greenhouse Gases NH_3, NO_2 and Cl_2: A DFT Study. *Mater. Today Chem.* **2024**, *38*, 102114. [CrossRef]
169. Chen, L.; Song, Y.; Yu, Q.; Dong, H.; Pan, C.; Wang, D.; Liu, J.; Chen, X. High-Performance Acetone Sensor Based on Electrospun Tb-Doped α-Fe_2O_3 Nanotubes. *Ceram. Int.* **2022**, *48*, 26828–26835. [CrossRef]
170. Cui, X.; Lu, Z.; Wang, Z.; Zeng, W.; Zhou, Q. Highly Sensitive SF_6 Decomposition Byproducts Sensing Platform Based on CuO/ZnO Heterojunction Nanofibers. *Chemosensors* **2023**, *11*, 58. [CrossRef]
171. Han, W.; Yang, J.; Jiang, B.; Wang, X.; Wang, C.; Guo, L.; Sun, Y.; Liu, F.; Sun, P.; Lu, G. Conductometric ppb-Level CO Sensors Based on In_2O_3 Nanofibers Co-Modified with Au and Pd Species. *Nanomaterials* **2022**, *12*, 3267. [CrossRef]
172. Hong, S.-Z.; Huang, Q.-Y.; Wu, T.-M. Facile Synthesis of Polyaniline/Carbon-Coated Hollow Indium Oxide Nanofiber Composite with Highly Sensitive Ammonia Gas Sensor at the Room Temperature. *Sensors* **2022**, *22*, 1570. [CrossRef] [PubMed]
173. Naresh, B.; Krishna, K.G.; Rajasekhar, D.; Kuchi, C.; Kummara, S.K.; Reddy, P.S. Synthesis and Characterization of rGO Wrapped 1-D NiO Nanofibers for Ammonia Gas Sensing Application. *Surf. Interfaces* **2023**, *40*, 103012. [CrossRef]
174. Fan, S.X.; Tang, W. Synthesis, Characterization and Mechanism of Electrospun Carbon Nanofibers Decorated with ZnO Nanoparticles for Flexible Ammonia Gas Sensors at Room Temperature. *Sens. Actuators B Chem.* **2022**, *362*, 131789. [CrossRef]
175. Cai, Z.; Park, S. Ultrasensitive Hydrogen Sensor Based on Porous-Structured Pd-Decorated In_2O_3 Nanoparticle-Embedded SnO_2 Nanofibers. *Sens. Actuators B Chem.* **2022**, *367*, 132090. [CrossRef]
176. Konuk Ege, G.; Akay, Ö.; Yüce, H. A Chemosensitive Based Ammonia Gas Sensor with PANI/PEO- ZnO Nanofiber Composites Sensing Layer. *MI* **2023**, in press. [CrossRef]
177. Lee, J.-H.; Kim, J.-Y.; Mirzaei, A.; Kim, H.W.; Kim, S.S. Significant Enhancement of Hydrogen-Sensing Properties of ZnO Nanofibers through NiO Loading. *Nanomaterials* **2018**, *8*, 902. [CrossRef]

178. Zhang, Q.; Wang, X.; Fu, J.; Liu, R.; He, H.; Ma, J.; Yu, M.; Ramakrishna, S.; Long, Y. Electrospinning of Ultrafine Conducting Polymer Composite Nanofibers with Diameter Less than 70 Nm as High Sensitive Gas Sensor. *Materials* **2018**, *11*, 1744. [CrossRef]
179. Fan, C.; Sun, F.; Wang, X.; Huang, Z.; Keshvardoostchokami, M.; Kumar, P.; Liu, B. Synthesis of ZnO Hierarchical Structures and Their Gas Sensing Properties. *Nanomaterials* **2019**, *9*, 1277. [CrossRef]
180. Liu, P.; Wu, S.; Zhang, Y.; Zhang, H.; Qin, X. A Fast Response Ammonia Sensor Based on Coaxial PPy–PAN Nanofiber Yarn. *Nanomaterials* **2016**, *6*, 121. [CrossRef]
181. Liu, H.; Wang, F.; Hu, K.; Zhang, B.; He, L.; Zhou, Q. Superior Hydrogen Sensing Property of Porous NiO/SnO_2 Nanofibers Synthesized via Carbonization. *Nanomaterials* **2019**, *9*, 1250. [CrossRef]
182. Ning, X.; Tang, D.; Zhang, M. Directly Electrospinning Submillimeter Continuous Fibers on Tubes to Fabricate H_2S Detectors with Fast and High Response. *Nano Mater. Sci.* **2022**, *4*, 376–382. [CrossRef]
183. Nair, K.G.; Vishnuraj, R.; Pullithadathil, B. Integrated Co-Axial Electrospinning for a Single-Step Production of 1D Aligned Bimetallic Carbon fibers@AuNPs–PtNPs/NiNPs–PtNPs towards H_2 Detection. *Mater. Adv.* **2022**, *3*, 443–455. [CrossRef]
184. Phuoc, P.H.; Hung, C.M.; Van Toan, N.; Van Duy, N.; Hoa, N.D.; Van Hieu, N. One-Step Fabrication of SnO_2 Porous Nanofiber Gas Sensors for Sub-ppm H_2S Detection. *Sens. Actuators A Phys.* **2020**, *303*, 111722. [CrossRef]
185. Hwang, S.-H.; Kim, Y.K.; Hong, S.H.; Lim, S.K. Cu/CuO@ZnO Hollow Nanofiber Gas Sensor: Effect of Hollow Nanofiber Structure and p-n Junction on Operating Temperature and Sensitivity. *Sensors* **2019**, *19*, 3151. [CrossRef] [PubMed]
186. Busacca, C.; Donato, A.; Lo Faro, M.; Malara, A.; Neri, G.; Trocino, S. CO Gas Sensing Performance of Electrospun Co_3O_4 Nanostructures at Low Operating Temperature. *Sens. Actuators B Chem.* **2020**, *303*, 127193. [CrossRef]
187. Li, H.-M.; Li, G.-X.; Li, L. Comparative Investigation on Combustion Characteristics of ADN-Based Liquid Propellants in Inert Gas and Oxidizing Gas Atmospheres with Resistive Ignition Method. *Fuel* **2023**, *334*, 126742. [CrossRef]
188. Yoo, J.-M.; Lee, Y.-R.; Kim, D.; Jeong, M.-J.; Stockwell, W.R.; Kundu, P.K.; Oh, S.-M.; Shin, D.-B.; Lee, S.-J. New Indices for Wet Scavenging of Air Pollutants (O_3, CO, NO_2, SO_2, and PM_{10}) by Summertime Rain. *Atmos. Environ.* **2014**, *82*, 226–237. [CrossRef]
189. Li, Y.; Fan, B.; Deng, G.; Zhang, H.; Zhang, J.; Du, H.; Shi, K. Effect of NO_2 on SO_2–SO_4^{2-} Conversion in Atmosphere: Evidence from Long-Term Precipitation. *Atmos. Environ.* **2024**, *334*, 120707. [CrossRef]
190. Galvao, E.S.; Reis Junior, N.C.; Goulart, E.V.; Kumar, P.; Santos, J.M. Refining Children's Exposure Assessment to NO_2, SO_2, and O_3: Incorporating Indoor-to-Outdoor Concentration Ratios and Individual Daily Routine. *Chemosphere* **2024**, *364*, 143155. [CrossRef]
191. Van Hoang, N.; Duc, L.M.; Hiep, N.T.; Hung, N.M.; Nguyen, C.V.; Hung, P.T.; Hoat, P.D.; Vo, V.K.; Heo, Y.-W. Optimization of Synthesis Conditions and Sensing Performance of Electrospun $NiFe_2O_4$ Nanofibers for H_2S and NO_2 Detection. *J. Alloys Compd.* **2023**, *936*, 168276. [CrossRef]
192. Zhang, B.; Zhang, S.; Xia, Y.; Yu, P.; Xu, Y.; Dong, Y.; Wei, Q.; Wang, J. High-Performance Room-Temperature NO_2 Gas Sensor Based on Au-Loaded SnO_2 Nanowires under UV Light Activation. *Nanomaterials* **2022**, *12*, 4062. [CrossRef] [PubMed]
193. Saasa, V.; Orasugh, J.T.; Mwakikunga, B.; Ray, S.S. Electrospun rGO-PVDF/WO_3 Composite Fibers for SO_2 Sensing. *Mater. Sci. Semicond. Process.* **2024**, *181*, 108631. [CrossRef]
194. Vishnuraj, R.; Aleem, M.; Nair, K.G.; Pullithadathil, B. 1D Aligned, n–p and n–n Type ZnO Heterojunction Nanofibers for NO_2 Sensors: Exploration of Conduction Mechanism Using in Situ Impedance Spectroscopy. *Mater. Adv.* **2023**, *4*, 3010–3025. [CrossRef]
195. Zou, B.; Guo, Y.; Shen, N.; Xiao, A.; Li, M.; Zhu, L.; Wan, P.; Sun, X. Sulfophenyl-Functionalized Reduced Graphene Oxide Networks on Electrospun 3D Scaffold for Ultrasensitive NO_2 Gas Sensor. *Sensors* **2017**, *17*, 2954. [CrossRef]
196. Bonyani, M.; Zebarjad, S.M.; Janghorban, K.; Kim, J.-Y.; Kim, H.W.; Kim, S.S. Au-Decorated Polyaniline-ZnO Electrospun Composite Nanofiber Gas Sensors with Enhanced Response to NO_2 Gas. *Chemosensors* **2022**, *10*, 388. [CrossRef]
197. Qiu, Y.; Wang, Y. Synthesis, Growth Kinetics and Ultra-Sensitive Performance of Electrospun WO_3 Nanofibers for NO_2 Detection. *Appl. Surf. Sci.* **2023**, *608*, 155112. [CrossRef]
198. Lahlou, H.; Claramunt, S.; Monereo, O.; Prades, D.; Fernandez-Sanjuá, J.-M.; Bonet, N.; Ramos, F.-M.; Cirera, A. Preparation of Palladium Oxide Nanoparticles Supported on Tin Oxide Nanofibers via Modified Electrospinning for Ultra-Low ppb NO_2 Detection. *Mater. Today Proc.* **2021**, *36*, 1–9. [CrossRef]
199. Guo, J.; Li, W.; Zhao, X.; Hu, H.; Wang, M.; Luo, Y.; Xie, D.; Zhang, Y.; Zhu, H. Highly Sensitive, Selective, Flexible and Scalable Room-Temperature NO_2 Gas Sensor Based on Hollow SnO_2/ZnO Nanofibers. *Molecules* **2021**, *26*, 6475. [CrossRef]
200. Khalifa, M.; Anandhan, S. Highly Sensitive and Wearable NO_2 Gas Sensor Based on PVDF Nanofabric Containing Embedded Polyaniline/g-C_3N_4 Nanosheet Composites. *Nanotechnology* **2021**, *32*, 485504. [CrossRef]
201. Morais, P.V.; Suman, P.H.; Silva, R.A.; Orlandi, M.O. High Gas Sensor Performance of WO_3 Nanofibers Prepared by Electrospinning. *J. Alloys Compd.* **2021**, *864*, 158745. [CrossRef]
202. Viet, N.N.; Thong, L.V.; Dang, T.K.; Phuoc, P.H.; Chien, N.H.; Hung, C.M.; Hoa, N.D.; Van Duy, N.; Van Toan, N.; Son, N.T.; et al. MoS_2 Nanosheets-Decorated SnO_2 Nanofibers for Enhanced SO_2 Gas Sensing Performance and Classification of CO, NH_3 and H_2 Gases. *Anal. Chim. Acta* **2021**, *1167*, 338576. [CrossRef] [PubMed]
203. Zhang, X.; Zhai, Z.; Wang, J.; Hao, X.; Sun, Y.; Yu, S.; Lin, X.; Qin, Y.; Li, C. Zr-MOF Combined with Nanofibers as an Efficient and Flexible Capacitive Sensor for Detecting SO_2. *ChemNanoMat* **2021**, *7*, 1117–1124. [CrossRef]
204. Wang, Y.; Chen, Z.; Chen, Q.; Tian, E.; Han, N.; Mo, J. Preconcentrating Sensor Systems toward Indoor Low-Concentration VOC Detection by Goal-Oriented, Sequential, Inverse Design Strategy. *Build. Environ.* **2024**, *254*, 111372. [CrossRef]

205. Zhao, Q.; Li, Y.; Chai, X.; Xu, L.; Zhang, L.; Ning, P.; Huang, J.; Tian, S. Interaction of Inhalable Volatile Organic Compounds and Pulmonary Surfactant: Potential Hazards of VOCs Exposure to Lung. *J. Hazard. Mater.* **2019**, *369*, 512–520. [CrossRef]
206. Zhang, F.; Wang, M.; Wang, M.; Fan, C.; Tao, L.; Ma, W.; Sui, S.; Liu, T.; Jia, L.; Guo, X. Revealing the Dual Impact of VOCs on Recycled Rubber Workers: Health Risk and Odor Perception. *Ecotoxicol. Environ. Saf.* **2024**, *283*, 116824. [CrossRef] [PubMed]
207. Ren, Y.; Guan, X.; Peng, Y.; Gong, A.; Xie, H.; Chen, S.; Zhang, Q.; Zhang, X.; Wang, W.; Wang, Q. Characterization of VOC Emissions and Health Risk Assessment in the Plastic Manufacturing Industry. *J. Environ. Manag.* **2024**, *357*, 120730. [CrossRef]
208. Zhu, L.; Wang, Z.; Wang, J.; Liu, J.; Zhang, J.; Yan, W. Pt-Embedded Metal–Organic Frameworks Deriving Pt/ZnO-In_2O_3 Electrospun Hollow Nanofibers for Enhanced Formaldehyde Gas Sensing. *Chemosensors* **2024**, *12*, 93. [CrossRef]
209. Ma, S.; Guo, J.; Zhang, H.; Shao, X.; Zhang, D. A Room Temperature Trimethylamine Gas Sensor Based on Electrospinned Molybdenum Oxide Nanofibers/$Ti_3C_2T_x$ MXene Heterojunction. *Nanomaterials* **2024**, *14*, 537. [CrossRef]
210. Liu, X.; Zhang, J.; Zhang, H.; Chen, C.; Zhang, D. Enhanced Sensing Performance of Electrospun Tin Dioxide Nanofibers Decorated with Cerium Dioxide Nanoparticles for the Detection of Liquefied Petroleum Gas. *Chemosensors* **2022**, *10*, 497. [CrossRef]
211. Dong, S.; Jin, X.; Wei, J.; Wu, H. Electrospun $ZnSnO_3$/ZnO Composite Nanofibers and Its Ethanol-Sensitive Properties. *Metals* **2022**, *12*, 196. [CrossRef]
212. Qu, C.; Zhao, P.; Wu, C.; Zhuang, Y.; Liu, J.; Li, W.; Liu, Z.; Liu, J. Electrospun PAN/PANI Fiber Film with Abundant Active Sites for Ultrasensitive Trimethylamine Detection. *Sens. Actuators B Chem.* **2021**, *338*, 129822. [CrossRef]
213. Cui, S.; Qin, J.; Liu, W. Ultrafine Pt-Doped SnO_2 Mesopore Nanofibers-Based Gas Sensor for Enhanced Acetone Sensing. *Chin. J. Anal. Chem.* **2023**, *51*, 100188. [CrossRef]
214. Du, H.; Li, X.; Yao, P.; Wang, J.; Sun, Y.; Dong, L. Zinc Oxide Coated Tin Oxide Nanofibers for Improved Selective Acetone Sensing. *Nanomaterials* **2018**, *8*, 509. [CrossRef] [PubMed]
215. Kim, J.-H.; Abideen, Z.; Zheng, Y.; Kim, S. Improvement of Toluene-Sensing Performance of SnO_2 Nanofibers by Pt Functionalization. *Sensors* **2016**, *16*, 1857. [CrossRef] [PubMed]
216. Prabhu, N.N.; Shivamurthy, B.; Anandhan, S.; Rajendra, B.V.; Basanna, J.C.R.; Srivathsa, M. An Investigation on the Acetone and Ethanol Vapor-Sensing Behavior of Sol–Gel Electrospun ZnO Nanofibers Using an Indigenous Setup. *ACS Omega* **2023**, *8*, 49057–49066. [CrossRef]
217. Baek, J.W.; Han, S.; Lee, S.E.; Ahn, J.; Park, C.; Nam, J.S.; Kim, Y.H.; Shin, E.; Kim, M.; Jang, J.-S.; et al. Cobalt-Doped Ceria Sensitizer Effects on Metal Oxide Nanofibers: Heightened Surface Reactivity for High-Performing Chemiresistive Sensors. *ACS Nano* **2024**, acsnano.4c03168. [CrossRef]
218. Zhang, J.; Lu, H.; Lu, H.; Li, G.; Gao, J.; Yang, Z.; Tian, Y.; Zhang, M.; Wang, C.; He, Z. Porous Bimetallic Mo-W Oxide Nanofibers Fabricated by Electrospinning with Enhanced Acetone Sensing Performances. *J. Alloys Compd.* **2019**, *779*, 531–542. [CrossRef]
219. Vu, D.L.; Lin, T.-F.; Lin, T.-H.; Wu, M.-C. Highly-Sensitive Detection of Volatile Organic Compound Vapors by Electrospun PANI/P3TI/PMMA Fibers. *Polymers* **2020**, *12*, 455. [CrossRef]
220. Can, N. Electrospun CuO Nanofibers for Room Temperature Volatile Organic Compound Sensing Applications. *Mater. Chem. Phys.* **2018**, *213*, 6–13. [CrossRef]
221. Hu, Q.; Huang, B.; Li, Y.; Zhang, S.; Zhang, Y.; Hua, X.; Liu, G.; Li, B.; Zhou, J.; Xie, E.; et al. Methanol Gas Detection of Electrospun CeO_2 Nanofibers by Regulating Ce^{3+}/ Ce^{4+} Mole Ratio via Pd Doping. *Sens. Actuators B Chem.* **2020**, *307*, 127638. [CrossRef]
222. Mehrabi, P.; Hui, J.; Janfaza, S.; O'Brien, A.; Tasnim, N.; Najjaran, H.; Hoorfar, M. Fabrication of SnO_2 Composite Nanofiber-Based Gas Sensor Using the Electrospinning Method for Tetrahydrocannabinol (THC) Detection. *Micromachines* **2020**, *11*, 190. [CrossRef] [PubMed]
223. Kishore, K.R.; Teddu, L.B.; Balamurugan, D.; Gopalakrishnan, J.B. Electrospun Co_3O_4 Nanoparticles and Its Methanol Detection Property. *Appl. Nanosci.* **2021**, *11*, 637–655. [CrossRef]
224. Joke, O.F.; Rotimi, I.A.; Makhatha, M.E.; Olaoye, O.P.; Yetunde, S.A.; Joy, O.O.; Victoria, O.T.; Bayode, A.T.; Ayantunde, A.A. Investigation of the Gas Sensing Potential of Electrospun Expanded Polystyrene/Reduced Graphene Oxide Nanofiber Composites. In *Chemical and Materials Sciences—Developments and Innovations*; Bhowmik, P.K., Ed.; B P International: Hooghly, West Bengal, India, 2024; Volume 2, pp. 1–17. [CrossRef]
225. Sun, Y.; Wang, Z.; Wang, W.; Li, G.; Li, P.; Lian, K.; Zhang, W.; Zhuiykov, S.; Hu, J.; Chen, L. Electrospinning Preparation of Pd@Co_3O_4-ZnO Composite Nanofibers and Their Highly Enhanced VOC Sensing Properties. *Mater. Res. Bull.* **2019**, *109*, 255–264. [CrossRef]
226. Shi, J.; Xu, C.; Han, Y.; Han, H. Enhanced Anaerobic Degradation of Nitrogen Heterocyclic Compounds with Methanol, Sodium Citrate, Chlorella, Spirulina, and Carboxymethylcellulose as Co-Metabolic Substances. *J. Hazard. Mater.* **2020**, *384*, 121496. [CrossRef]
227. Khot, L.R.; Panigrahi, S.; Sengupta, P. Development and Evaluation of Chemoresistive Polymer Sensors for Low Concentration Detection of Volatile Organic Compounds Related to Food Safety Applications. *Sens. Instrumen. Food Qual.* **2010**, *4*, 20–34. [CrossRef]
228. Jenkins, J.D.; Luke, M.; Thernstrom, S. Getting to Zero Carbon Emissions in the Electric Power Sector. *Joule* **2018**, *2*, 2498–2510. [CrossRef]
229. Sun, X.; Tang, M.; Yu, M.; Fan, Y.; Qin, C.; Cao, J.; Wang, Y. UV-Activated CH_4 Gas Sensor Based on Pd@Ni/ZnO Microspheres. *Mater. Today Commun.* **2024**, *40*, 109551. [CrossRef]

230. Lai, T.-Y.; Fang, T.-H.; Hsiao, Y.-J.; Chan, C.-A. Characteristics of Au-Doped SnO_2–ZnO Heteronanostructures for Gas Sensing Applications. *Vacuum* **2019**, *166*, 155–161. [CrossRef]
231. Zhang, Q.; Liang, S.-X.; Jia, Z.; Zhang, W.; Wang, W.; Zhang, L.-C. Efficient Nanostructured Heterogeneous Catalysts by Electrochemical Etching of Partially Crystallized Fe-Based Metallic Glass Ribbons. *J. Mater. Sci. Technol.* **2021**, *61*, 159–168. [CrossRef]
232. Han, Y.; Zhang, F.; Gong, H.; Cai, C. Functional Three Helix Molecular Beacon Fluorescent "Turn-on" Probe for Simple and Sensitive Simultaneous Detection of Two HIV DNAs. *Sens. Actuators B Chem.* **2019**, *281*, 303–310. [CrossRef]
233. Staerz, A.F.; Seo, H.G.; Tuller, H.L. Surface Electron Modulation of Metal Oxide-based Electrochemical Devices by Surface Additives—Linking Sensors and Fuel Cells. *J. Am. Ceram. Soc.* **2024**, *107*, 1959–1973. [CrossRef]
234. Mokrushin, A.S.; Nagornov, I.A.; Simonenko, T.L.; Simonenko, N.P.; Gorobtsov, P.Y.; Arkhipushkin, I.A.; Simonenko, E.P.; Sevastyanov, V.G.; Kuznetsov, N.T. Gas-Sensitive Nanostructured ZnO Films Praseodymium and Europium Doped: Electrical Conductivity, Selectivity, Influence of UV Irradiation and Humidity. *Appl. Surf. Sci.* **2022**, *589*, 152974. [CrossRef]
235. Mo, X.; Zhu, C.; Zhang, Z.; Yan, X.; Han, C.; Li, J.; Attfield, J.P.; Yang, M. Nitrogen-Doped Indium Oxide Electrochemical Sensor for Stable and Selective NO_2 Detection. *Adv. Mater.* **2024**, *36*, 2409294. [CrossRef] [PubMed]
236. Lei, L.; Xie, W.; Chen, Z.; Jiang, Y.; Liu, Y. Metal Ion Chelation-Based Color Generation for Alkaline Phosphatase-Linked High-Performance Visual Immunoassays. *Sens. Actuators B Chem.* **2018**, *273*, 35–40. [CrossRef]
237. Suh, J.M.; Lee, T.H.; Hong, K.; Song, Y.G.; Cho, S.H.; Kang, C.-Y.; Shim, Y.-S.; Lee, D.; Kwon, K.C.; Jang, H.W. Extremely Sensitive and Selective NO_2 Detection at Relative Humidity 90% in 2-Dimensional Tin Sulfides/SnO_2 Nanorod Heterostructure. *Sens. Actuators B Chem.* **2022**, *369*, 132319. [CrossRef]
238. Bhatia, A.; Na, H.S.; Nandhakumar, P.; Yu, B.; Jon, S.; Chung, J.; Yang, H. Electrochemical Detection of Interleukin-8 in Human Saliva Using a Polyenzyme Label Based on Diaphorase and Neutravidin. *Sens. Actuators B Chem.* **2021**, *326*, 128979. [CrossRef]